Title

Improving snow albedo processes in WRF/SSiB regional climate model to assess impact of dust and black carbon in snow on surface energy balance and hydrology over western U.S.

Journal

Journal of Geophysical Research, 120(8)

ISSN

0148-0227

Authors

Oaida, CM
Xue, Y
Flanner, MG
et al.

Publication Date

2015

DOI

10.1002/2014JD022444

Peer reviewed

AGU PUBLICATIONS

JGR

Journal of Geophysical Research: Atmospheres

RESEARCH ARTICLE
10.1002/2014JD022444

Key Points:
- Including snow aging and aerosols in snow improves offline and WRF snow simulations
- Dust and black/organic carbon exerts nontrivial radiative forcing in western U.S.
- RCM simulation shows temperature increase and snow mass loss from aerosols in snow

Correspondence to:
C. M. Oaida,
oaidac@ucla.edu

Citation:
Oaida, C. M., Y. Xue, M. G. Flanner, S. M. Skiles, F. De Sales, and T. H. Painter (2015), Improving snow albedo processes in WRF/SSiB regional climate model to assess impact of dust and black carbon in snow on surface energy balance and hydrology over western U.S., *J. Geophys. Res. Atmos.*, *120*, 3228–3248, doi:10.1002/2014JD022444.

Received 15 AUG 2014
Accepted 23 FEB 2015
Accepted article online 26 FEB 2015
Published online 27 APR 2015

Improving snow albedo processes in WRF/SSiB regional climate model to assess impact of dust and black carbon in snow on surface energy balance and hydrology over western U.S.

Catalina M. Oaida[1], Yongkang Xue[1,2], Mark G. Flanner[3], S. McKenzie Skiles[2], Fernando De Sales[2], and Thomas H. Painter[2,4]

[1]Department of Atmospheric and Oceanic Sciences, University of California, Los Angeles, California, USA, [2]Department of Geography, University of California, Los Angeles, California, USA, [3]Department of Atmospheric, Oceanic and Space Sciences, University of Michigan, Ann Arbor, Michigan, USA, [4]Jet Propulsion Laboratory/California Institute of Technology, California, USA

Abstract Two important factors that control snow albedo are snow grain growth and presence of light-absorbing impurities (aerosols) in snow. However, current regional climate models do not include such processes in a physically based manner in their land surface models. We improve snow albedo calculations in the Simplified Simple Biosphere (SSiB) land surface model coupled with the Weather Research and Forecasting (WRF) regional climate model (RCM), by incorporating the physically based SNow ICe And Radiative (SNICAR) scheme. SNICAR simulates snow albedo evolution due to snow aging and presence of aerosols in snow. The land surface model is further modified to account for deposition, movement, and removal by meltwater of such impurities in the snowpack. This paper presents model development technique, validation with in situ observations, and preliminary results from RCM simulations investigating the impact of such impurities in snow on surface energy and water budgets. By including snow-aerosol interactions, the new land surface model is able to realistically simulate observed snow albedo, snow grain size, dust in snow, and surface water and energy balances in offline simulations for a location in western U.S. Preliminary results with the fully coupled RCM show that over western U.S., realistic aerosol deposition in snow induces a springtime average radiative forcing of 16 W/m^2 due to a 6% albedo reduction, a regional surface warming of 0.84°C, and a snowpack reduction of 11 mm.

1. Introduction

1.1. Snow and Aerosols in Snow

Snow plays a significant role in Earth's surface energy and water budgets. Changes to its albedo influence snowmelt and snow cover extent, impacting the strength of the snow-albedo feedback, and therefore climate [e.g., *Budyko*, 1969; *Yang et al*., 2001; *Xue et al*., 2003; *Qu and Hall*, 2007; *Flanner et al*., 2007]. Additionally, changes in snowmelt affect runoff, which is important from a water resources perspective [*Leung et al*., 2003; *Painter et al*., 2010]. Many factors, including snow grain size and impurities in snow, influence snow albedo [*Wiscombe and Warren*, 1980; *Warren and Wiscombe*, 1980]. With older, larger snow grains, the path length of radiation passing through the grain is larger, thus increasing the probability that a photon will be absorbed, which would lead to the lowering of snow albedo [*Wiscombe and Warren*, 1980]. Additionally, light-absorbing impurities in snow such as mineral desert dust and black carbon (BC) can drastically reduce its albedo, especially in the visible part of the spectrum [*Warren and Wiscombe*, 1980]. Aerosols in snow can lower surface albedo threefold through its radiative forcing effects: due to the presence of the aerosol itself in the snow (direct effect), by causing larger snow grains due to accelerated snow metamorphism from snowpack heating (first indirect effect), and by exposing darker substrate earlier due to the previous two effects (second indirect effect) [*Hansen and Nazarenko*, 2004]. These are often referred to as the radiative forcing of impurities in snow.

In situ observations, ice cores, and satellite imagery show that both dust and BC emissions and deposition onto mountain snowpacks world-wide have increased, primarily due to human activity [e.g., *Belnap and Gillette*, 1998; *Thompson et al*., 2000; *Liu et al*., 2007; *Neff et al*., 2008; *Ming et al*., 2008; *Xu et al*., 2009].

Regionally, in areas like southwest U.S., studies have found that disturbed soils due to grazing by domestic livestock consistently produced more sediment (2.8 times more) than undisturbed soils [*Belnap et al*., 2009], increasing dust emission from those areas. Reduced plant cover during drought years also impacts soil surface stability and therefore dust emissions. In congruence with this observed dust emission increase, dust deposition at alpine sites in this region, particularly in the southern Rocky Mountains, has also increased [*Neff et al*., 2008; *Painter et al*., 2012; *Li et al*., 2013]. On the other hand, BC emission in western U.S. (WUS) occurs primarily close to urban centers [e.g., *Bond et al*., 2007], but the largest impact would take place where urban areas and snow intersect most. BC deposition on snow is highly influenced by orographic effects [e.g., *Qian et al*., 2009], but deposition in snow from dead trees from old forest fires has also been observed [e.g., *Sterle et al*., 2013; *Gleason and Nolin*, 2013].

1.2. Need for Regional Climate Models (RCMs) With Physically Based Snow Models for Regional Studies

Sensitivity studies have shown that impurities in snow such as dust and BC, by changing albedo, have an impact on snow melt timing and amount [e.g., *Flanner et al*., 2007; *Qian et al*., 2009; *Painter et al*., 2010], and are more efficient at melting snow than warmer surface air temperatures [*Hansen and Nazarenko*, 2004; *Hansen et al*., 2005; *Flanner et al*., 2009; *Qian et al*., 2011; *Skiles et al*., 2012]. Previous studies found that BC in snow has a non-negligible climate forcing, impacting surface temperature [*Hansen and Nazarenko*, 2004], causing peak runoff to occur earlier than if snow was clean [*Flanner et al*., 2007]. These provide a first estimate of potential impacts of aerosols in snow. However, because global circulation models (GCMs) are used in these studies, they cannot resolve orographic-related precipitation processes due to coarser spatial resolution and smoother terrain, and therefore perform poorly when simulating snow in areas of complex topography [*Ghan and Shippert*, 2006; *Christensen et al*., 2007], such as the WUS.

It is important to better understand and quantify the impact of aerosols in snow on the mountain snowpack and on subsequent hydrologic cycle, atmospheric circulation, and climate, especially at a regional scale, since that is the scale at which resource managers, policy makers, and stakeholders are most concerned. Appropriate spatial resolution using regional climate models (RCMs) can improve snow simulations because they can more realistically reproduce orographic precipitation and snowpack accumulation over regions of complex topography such as the WUS [*Leung et al*., 2003; *Leung and Qian*, 2003; *Rasmussen et al*., 2011]. *Qian et al*. [2009] used an RCM in a sensitivity study over WUS to investigate the impact of BC on the hydrologic cycle. However, this study did not consider snow aging or vertically resolved snowpack radiative heating processes, including those due to aerosols in snow. These processes have been shown to be important to snow-albedo evolution and ice-albedo feedback [*Marbouty*, 1980; *Fukuzawa and Akitaya*, 1993; *Sturm and Benson*, 1997; *Flanner and Zender*, 2005, 2006]. Representation of light-absorbing impurities in snow, snow aging, and vertically resolved snowpack radiative transfer processes allows models to capture the amplifying effect of aerosols in snow.

Up until recently, there were no comprehensive regional studies using RCMs with physically based snow schemes that consider snow aging, interactive snow radiative transfer, and presence of aerosols in snow, primarily due to a lack of models that account for such processes. We have modified and enhanced a land surface-regional climate model where the end product is one of few models that can be used at local and regional scales to quantitatively assess the impact of light-absorbing impurities such as dust, BC, and organic carbon (OC) in snow on regional mountain snowpack and associated hydrologic cycle, as well as possible impacts on regional climate due to their radiative forcing. To achieve this, we coupled the SNow ICe and Aerosol Radiative (SNICAR) model [*Flanner and Zender*, 2005, 2006; *Flanner et al*., 2007, 2009; *Oleson et al*., 2010], a physically based snow scheme that includes snow aging and aerosols in snow when computing snow albedo, into the Simplified Simple Biosphere model version 3 (SSiB-3), which has already been incorporated within a regional climate model (namely, WRF-ARW). The model is modified such that SNICAR snow albedo is used in the SSiB-3 surface albedo and snow energy and water balance calculations. Additionally, a new scheme is designed to allow for the input to, movement within, and removal from the snowpack of aerosols such as dust, BC, and OC. The development of the new model is detailed in this paper, along with its validation and preliminary results of its full potential application. Our focus is on WUS where observed dust deposition on the Rocky Mountains snowpack is of great concern since mountain snowmelt supports irrigation, hydropower generation, and nearly 40 million people across seven states in this area (Colorado River Basin Water Supply and Demand Study, U.S. Department of Interior Bureau of Reclamation, 2012, http://www.usbr.gov/lc/region/programs/

crbstudy/finalreport/index.html). However, the model can be employed at varying spatial resolutions, from 1 to 90 km, and its output could be used in hydrologic models for various local and regional applications.

2. Model Description

2.1. Regional Climate Model/Land Surface Model (WRF/SSiB-3)

The regional climate model (RCM) used in this work is the Weather Research and Forecasting/Advanced Research WRF (WRF-ARW) v3.2 model [*Shamarock et al*., 2008]. WRF-ARW is able to resolve topographic features such as the Rocky Mountains in WUS when run at a higher resolution such as 15 km, which results in a realistic simulation of orographic precipitation and snowpack spatial variability when compared to observations [*Qian et al*., 2010; *Rasmussen et al*., 2011]. The Simplified Simple Biosphere version 3 (SSiB-3) [*Xue et al*., 1991, 2003] land surface model is employed, which is a biophysically based model that simulates land-atmosphere interactions by calculating the surface energy budget and surface water balance for three soil layers and one vegetation layer, with snow processes simulated by the Snow-Atmosphere-Soil Transfer scheme [*Sun et al*., 1999; *Xue et al*., 2003]. SSiB-3 has been validated with observational data, as well as in snow-model intercomparisons [e.g., *Xue et al*., 2003; *Rutter et al*., 2009; *Shrestha et al*., 2012]. SSiB has been coupled with a number of RCMs to extensively conduct U.S. regional climate studies [e.g., *Xue et al*., 2001, 2007; *De Sales and Xue*, 2012], and the version integrated with WRF-ARW, hereinafter referred to as (WRF/SSiB-3), has been released for public use through the National Center For Atmospheric Research WRF website.

In SSiB-3, precipitation is categorized as snow when it accumulates with the surface air temperature below 0°C. Snow can accumulate on both the vegetation canopy and the ground, where the snowpack is one bulk layer if the snow is less than 7 cm, or three layers if it is thicker than 7 cm (see section A1 in Appendix A for more details on snow layer subdivision in SSiB-3). Snow cover fraction is determined based on snow depth, which can be decreased by compaction and melting, and increased by new snow. This snow cover scheme is similar to the SIB2/CSU parameterization [*Sellers et al*., 1996]. Changes in snow water equivalent (SWE), which is the sum of liquid water and ice grain mass, are described by the mass balance, with precipitation, snow melting, and evaporation/sublimation at the snow surface being the main contributors. In the original SSiB-3 and WRF/SSiB-3, *surface* albedo is calculated based on canopy and ground-level albedos, weighted by vegetation cover fraction (VCF):

$$\alpha_{\text{surface}} = \alpha_{\text{canopy}} \times \text{VCF} + \alpha_{\text{ground}} \times (1 - \text{VCF}), \tag{1}$$

where α_{canopy} and α_{ground} are each calculated for diffuse and direct, VIS and NIR radiation. α_{canopy} considers vegetation and snow-on-vegetation reflectance in the radiative transfer calculations. For α_{ground}, snow cover fraction (SCF) is also considered, to differentiate between snow-covered and snow-free areas, and for the latter, whether there is vegetation or not:

$$\alpha_{\text{ground}} = \text{SCF} \times \alpha_{\text{snow}} + (1 - \text{SCF}) \times \left[(1 - \text{VCF}) \times \alpha_{\text{soil}} + \text{VCF} \times \alpha_{\text{vegetation}}\right], \tag{2}$$

In this original version of SSiB-3, snow albedo (α_{snow}) is parameterized and related to SCF and solar zenith angle. If melting occurs within the snowpack, snow albedo in this pre-modified version of SSiB-3 is reduced empirically by 60% of the fresh snow albedo (0.85 in visible, 0.65 in near infrared). For this work, we replace the original α_{snow} in the α_{canopy} and α_{ground} calculations with a more physically based snow albedo, as described in the following section.

The already integrated regional climate model (WRF-ARW)-land surface model (SSiB-3) just described will hereinafter be referred to as WRF/SSiB-3/orig, representing the original model.

2.2. New Snow Processes in WRF/SSiB-3

In this work, we coupled the SNow ICe and Aerosol Radiative (SNICAR) model by *Flanner and Zender* [2005, 2006] into the WRF/SSiB-3/orig regional climate model (Figure 1). Here we employ the multi-layer coupled snow aging and radiative transfer schemes that are implemented in the Community Land Model (CLM)/CESM-GCM framework, described in detail by *Oleson et al*. [2010], rather than the pure radiative transfer implementation of SNICAR that is available on the web at http://snow.engin.umich.edu/. SNICAR simulates radiative transfer in the snowpack using the two-stream, multiple scattering, multi-layer radiative approximation of *Toon et al*. [1989]. Optical properties of ice grains and light-absorbing impurities are calculated with Mie theory on the

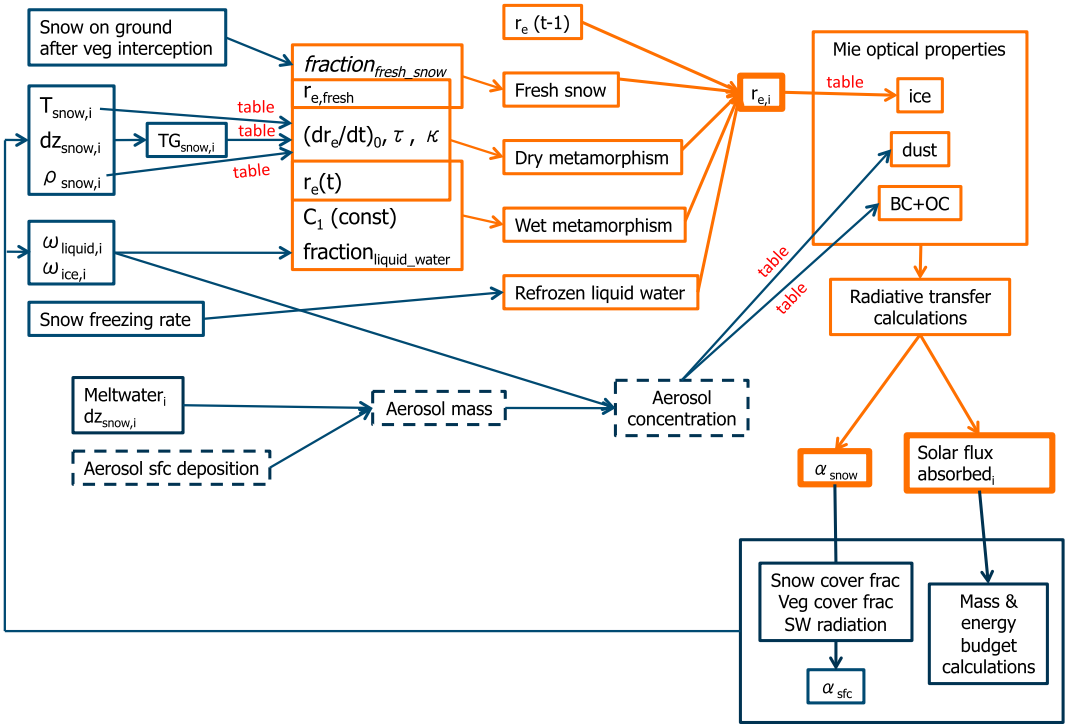

Figure 1. Schematic diagram for coupling of SNICAR into SSiB-3 land surface model (LSM). Variables defined in text. Blue boxes represent LSM variables or processes; orange boxes represent SNICAR variables or processes. Dashed blue boxes indicate variables or processes added to, or modified in, LSM to create new model. Bolded boxes indicate main SNICAR outputs, critical to improvements made in the model. "Table" refers to the fact that a lookup table computed offline is used to extract necessary information. See text for full description of SNICAR/SSiB-3 processes and integration.

same five-band spectral grid employed by the radiative transfer model. Ice optical properties depend on the snow effective grain size, which is prognosed by the snow aging scheme described next.

2.2.1. Snow Grain Growth

SNICAR calculates the effective snow grain radius, representing the snow aging process, as a function of snow temperature T_{snow}, temperature gradient TG_{snow} between snow layers, and snow density ρ_{snow} based on an empirical equation by *Legagneux et al.* [2004], which robustly fits predictions of grain size evolution from a more detailed microphysical model [*Flanner and Zender*, 2006]. This equation represents dry metamorphism, or vapor diffusion due to vapor density gradients resulting from vertical temperature gradient and differences in curvature of the snow particles, two of the five processes believed to contribute to snow grain growth. Wet metamorphism is represented empirically based on *Brun* [1989]. Refreezing of liquid water and deposition of fresh snow also contribute to grain evolution, the latter being represented by effective radius of fresh snow. Sintering, the fifth process [e.g., *Zhang and Scneibel*, 1995; *Colbeck*, 2001; *Blackford*, 2007], is not explicitly modeled in this scheme but is implicitly accounted for, to some extent, in the aging parameters applied for dry snow evolution. Therefore, the effective snow grain radius, r_e, calculated by SNICAR at a given time t, is

$$r_e(t) = \left[r_e(t-1) + \left(\frac{dr_e}{dt}\right)_{dry} dt + \left(\frac{dr_e}{dt}\right)_{wet} dt \right] f_{old} + r_{e,refreeze} f_{refreeze} + r_{e,fresh\_snow} f_{fresh\_snow} \quad (3)$$

where $r_e(t-1)$ is the effective grain radius at the previous time step,

$$\left(\frac{dr_e}{dt}\right)_{dry} = \left(\frac{dr_e}{dt}\right)_0 \left(\frac{\tau}{dr_{fresh\_snow} + \tau}\right)^{1/\kappa} \quad (4)$$

and

$$\left(\frac{dr_e}{dt}\right)_{wet} = \frac{10^{18} C_1 f_{liq}^3}{4\pi r_e^2} \quad (5)$$

are the change in snow radius due to dry metamorphism and wet metamorphism, respectively (see *Oleson et al.* [2010], for a description of SNICAR in CLM/CESM-GCM). $\left(\frac{dr_e}{dt}\right)_0$ is the initial rate of change of effective radius, dr_{fresh_snow} is the difference between $r_e(t-1)$ and that of fresh snow ($r_{e,fresh\_snow}$) — here $r_{e,fresh\_snow}$ is set to a constant value of 54 μm; τ and κ are best-fit parameters calculated offline and extracted from a lookup table based on snow temperature T_{snow}, snow temperature gradient TG_{snow}, and snow density ρ_{snow}; C_1 is a wet snow aging constant from *Brun* [1989], and f_{liq} is the liquid water fraction in snow ($fraction_{liquid\_water}$ in Figure 1). $r_{e,refreeze}$ is set to 1000 μm, $f_{refreeze}$ is the fraction of layer mass that is refrozen, and f_{new_snow} is the fraction of layer mass that is new snow. In the coupling of SNICAR with SSiB-3 (Figure 1), SSiB-3 provides input variables needed to calculate $r_{e,i}$ for each of the three snow layers i, namely, snow temperature ($T_{snow,i}$) and density ($\rho_{snow,i}$), snow layer thickness ($dz_{snow,i}$), liquid water ($\omega_{liquid,i}$) and ice ($\omega_{ice,i}$) contents in snow layer (from which snow temperature gradient is calculated), amount of snow on ground after interception by canopy, and snow refreezing rate, as illustrated in Figure 1. Because there is limited scientific literature and quantitative understanding about the process of refreezing, we chose to turn off the refreezing term in this study.

2.2.2. Radiative Transfer

Once the effective snow grain radius for each snow layer is computed, it is passed to the snow radiative transfer part of SNICAR, where it is used to select the appropriate Mie optical properties for ice. Optical properties (single scattering albedo ω, mass extinction cross-section, and asymmetry scattering parameter, g) are also determined for eight aerosol types (hydrophilic and hydrophobic BC, hydrophilic and hydrophobic organic carbon, and four dust particle sizes) using a lookup table computed offline. These optical properties are used along with the solar zenith angle, bare surface reflectance (α_{soil}), ice ($\omega_{ice,i}$) and liquid water ($\omega_{liquid,i}$) contents, and concentration of absorbing impurities (if present) provided by WRF/SSiB-3 (Figure 1) to calculate bulk snow albedo (α_{snow}) and absorbed solar radiation flux in each snow layer (solar flux $absorbed_i$) for visible and NIR bands, through a set of radiative transfer calculations.

2.2.3. SNICAR in SSiB-3

Output from the SNICAR radiative transfer scheme, namely, snow albedo and absorbed solar radiation by each snow layer, is passed back to SSiB-3. The original snow albedo, α_{snow}, described in section 2.1 that was calculated empirically is replaced by the snow grain size and impurities-dependent snow albedo calculated by SNICAR. The absorbed flux in each snow layer is used in SSiB-3 calculations of snow and surface/soil water and energy balances (Figure 1).

The SNICAR snow aging and snow radiative transfer schemes are employed by SSiB-3 twice, once for snow layer on the canopy and once for the snowpack on the ground. For each of these, SNICAR is called if the canopy or ground temperature, respectively, is less than 0°C and if SWE is greater than a minimum threshold, currently set to 1.0E−08 m (1.0E−05 mm). If temperature is below 0°C, and SWE is greater than zero but less than the minimum SWE, the effective snow grain radius is set to that of fresh snow and only the radiative transfer part of SNICAR is called. If the temperature is not below 0°C, or SWE is not greater than zero, SNICAR is not called. For the ground, r_e is computed as described above [equation (3)], while for the canopy level, the effective snow grain radius is always set to that of fresh snow because we assume snow does not get the chance to accumulate much before falling off the vegetation, and will thus be relatively new snow with smaller grains.

2.3. Tracking Aerosol Mass in the Model

Since the new snow scheme computes snow albedo based on optical properties of snow grains and aerosols present in snow, SSiB-3 was modified to account for the input and tracking of light-absorbing impurities within the modeled snowpack. Specifically, aerosol mass is first inputted into the model, provided either by an aerosol surface deposition map or by an atmospheric chemistry/transport model, and the sum of wet and dry surface aerosol deposition, D_m [kg/m^2], is added to the top snow layer only (Figure 1). *Mass concentration* (mixing ratio) [kg/kg] of aerosols is calculated and passed to the radiative transfer part of SNICAR, where it is used to calculate snow albedo and solar flux absorptance. The *mass of aerosols* [kg/m^2] is passed in the subroutine where SSiB-3 deals with melting in the snowpack in order to calculate possible scavenging of aerosols by meltwater. The mass rate of change of aerosols in each snow layer due to meltwater removal is

$$\frac{dm_i}{dt} = k\left(q_{i+1}c_{i+1} - q_i c_i\right) + D_m \tag{6}$$

where m_i is the mass of aerosol in layer i, k is the species-dependent scavenging ratio, derived from *Conway et al.* [1996] (see Table A1 in Appendix A), q_i is the mass flux of water out of layer i, and c_i is the mass mixing

Table 1a. List of Experiments Conducted, Respective Model Version Used, and Relevant Model Details Included

Simulation Type	Simulation Name	Model Used	Snow Aging	Aerosols in Snow
Offline	NOAER	SSiB-3/aer	Yes	No
	AER	SSiB-3/aer	Yes	Yes
Coupled/RCM	wrf_ORIG	WRF/SSiB-3/orig	No	No
	wrf_NOAER	WRF/SSiB-3/aer	Yes	No
	wrf_AER	WRF/SSiB-3/aer	Yes	Yes

ratio of aerosol in layer *i*. The *k* scavenging ratios used in this study (0.03 for hydrophobic BC and 0.2 for hydrophilic BC) from *Conway et al*. [1996] are broadly comparable to those derived more recently for BC in snow in Alaska by *Doherty et al*. [2013] (ranging 0.12 to 0.2). Some aerosol mass will be lost entirely from the snowpack when runoff from snowpack occurs. The aerosol mass rate of change due to meltwater removal was inspired by the method used in the Community Land Model [e.g., *Flanner et al*., 2007; *Oleson et al*., 2010]. Finally, a method was developed to allow aerosol mass within the snowpack to be adjusted based on the number of snow layers and how each snow layer thickness might change within a model time step due to new snowfall, compaction, and melt; both aerosol mass and snow layer depth are updated at every time step in SSiB-3 (see sections A1 and A2 in Appendix A for more details).

The enhanced WRF/SSiB-3 model, as described in this section and summarized in Figure 1, will hereinafter be referred to as WRF/SSiB-3/aer. Next section describes the experimental setup used to validate and utilize the new model.

3. Experiments and Data

Two types of experiments were conducted using the new model: (i) a set of point-based simulations using the offline version of the land surface model (SSiB-3/aer) and (ii) a set of regional simulations over WUS using the fully coupled WRF/SSiB-3/aer. The various experiments and models used are summarized in Tables 1a and 1b.

3.1. Offline Simulation

3.1.1. Experimental Design

The newly modified SSiB-3/aer is used to conduct a set of point-based simulations to help assess the model's performance in reproducing snow properties and processes, such as snow albedo and depth, dust distribution in snowpack, and snow grain size evolution, when compared to observations. The offline SSiB-3/aer model is run for four different years (2009, 2011, 2012, and 2013) for a location in the San Juan Mountains of the southern Rocky Mountains in WUS named Swamp Angel Study Plot (SASP) [see *Painter et al*., 2012, for more in depth site description]. SASP is a subalpine site located at 3371 m altitude in the eastern half of the Colorado River Basin at 37°54′N, 107°52′W. The measurements are taken in a sheltered clearing surrounded by subalpine forest. "Groundcover only" vegetation type is selected for the model simulation. SSiB-3/aer is run January through July (except for 2012 for when data were only available through May), under two different scenarios: (1) clean snow (NOAER)—no dust deposition, and (2) aerosol-loaded snow (AER)—observed levels of desert dust in snow used as forcing.

In addition, several sensitivity tests were performed to assess the model's response to uncertainties in dust forcing, such as those due to dust optical properties and amount of dust input. These experiments are summarized in Table 1b. Current SNICAR dust optical properties used in the snow radiative transfer part of the model are representative of dominant global dust. Our modeling study focuses on WUS, and dust in snow found in this region, where it has been found that using generic global dust optical properties cannot accurately

Table 1b. List of Sensitivity Tests Regarding Dust Optical Properties (Namely, Single Scattering Albedo, ω) and Dust Mass Input, and Corresponding Snow Depth Bias for Each Sensitivity Test With Respect to Snow Pit Observations Averaged Over the Ablation Period (15 Apr-SAG)[a]

	Optical Properties	Dust Input	Abs Bias
AER-st1	ω	Obs	0.103
AER-st2	ω	2X obs	0.071
AER-st3	ω-0.2	Obs	0.045
AER-st4	ω-0.2	2X obs	0.114

[a]Bias calculated using magnitude of OBS-MDL differences.

constrain the reduction in snow albedo due to dust, either in magnitude or reflectance shape [*Skiles*, 2014]. We therefore reduce ω by 0.2 as one of the sensitivity studies, to assess the impact of changing dust optical properties on simulated albedo and snow depth (test AER-st3). We also performed tests in which the amount of dust mass inputted is doubled from that observed for both original ω values scenario (test AER-st2) and reduced ω scenario (test AER-st4). AER-st1 is the simulation with the original ω values and observed dust mass as forcing. The main offline simulations for the 4 years at the SASP location (AER and NOAER) were conducted using $\omega - 0.2$ and observed amount of dust mass since we wanted to account for the more absorptive WUS dust [e.g., *Skiles*, 2014] while matching observed albedo and snow depth as best as possible (see section 4.1.3 under Results Analysis and Discussion, Figure 4, and Table 1b). In light of very recent results by *Skiles* [2014], where ω of WUS dust was determined to be lower than the global mean dust used in SNICAR by as much as 0.13 in the visible, reducing ω by 0.2 is a reasonable approach for this study, although work toward incorporating these new optical properties values within the SSiB-3/aer and WRF/SSiB-3/aer frameworks for use in WUS regional simulations is underway.

3.1.2. Data

The in situ measurements used here were acquired for the Integrated Hydrologic Response to Extreme Dust Deposition to the Snow Cover of the Colorado River Basin (IDS) project. A network of energy balance towers is being developed in the Colorado River Basin, with SASP in the Senator Beck Basin Study Area being fully functional since 2005. They have been operated by the Center for Snow and Avalanche Studies (CSAS) (www.snowstudies.org) in conjunction with the Snow Optics Laboratory at NASA/California Institute of Technology's Jet Propulsion Laboratory. Measurements from this site are described in detail and evaluated in *Painter et al*. [2012] and *Skiles et al*. [2012]. The meteorological measurements from these towers are used as input to drive the SSiB-3/aer model. Dust mass sampled from the snow column near the tower is also used as forcing. Dust was deposited onto snow in the model on the dates recorded as dust-on-snow deposition events by the CSAS and IDS programs. The amount of dust used in the model is a combination of in situ values recorded by CSAS and IDS on or near the dates of the dust events, depending on data availability. The CSAS data are from 0.5 m^2 area bulk measurements, while the IDS data are from 3 cm $\times$ 0.05 m^2 gravimetric samples collected across the top 30 cm of the snowpack. Dust events timing and magnitudes are indicated for reference in Figure 2 along with albedo.

3.2. RCM Simulations

3.2.1. Experimental Design

The ultimate goal is to use WRF/SSiB-3/aer at a regional scale to both achieve a more realistic simulation and help investigate more quantitatively the impact of aerosols in snow on snowpack state and related hydrologic processes at such scale. As a first step in reaching these goals, we conduct a preliminary study using the newly improved model, WRF/SSiB-3/aer, in the coupled mode over the WUS (see Figure 10 for model domain coverage). WRF/SSiB-3/aer is used under two different scenarios, clean (wrf_NOAER) and aerosol-loaded (wrf_AER) snow, at a spatial model resolution of 15 km, from January to July 2009 (see Table 1a). As in the offline simulations, ω values are reduced by 0.2 in these experiments to more closely represent WUS dust absorptive properties (see section 3.1.1).

3.2.2. Data

Global NCEP Reanalysis II product (http://nomad3.ncep.noaa.gov/ncep_data/index.html) is used as initial and lateral boundary conditions for both scenarios, while for the aerosol-loaded case, the GOCART aerosol deposition data set is also used as forcing. GOCART, the Goddard Chemistry Aerosol Radiation and Transport model, simulates emission, transport, and wet and dry deposition of major tropospheric aerosol components, including dust, BC, organic carbon (OC), sulfur, and sea salt [e.g., see *Chin et al*., 2000, for sulfate; *Ginoux et al*., 2001, for dust; and *Chin et al*., 2002, for other aerosols]. The model has been used in several studies to simulate dust distribution globally, and comparison with observations find that it generally reproduces dust distribution patterns and seasonal surface concentration variability reasonably well [e.g., *Ginoux et al*., 2001, 2004]. Using the GOCART aerosol deposition data allows us to apply a realistic spatial and temporal aerosol forcing on snow. For this work, the GOCART group provided monthly accumulations of these aerosols for 2009 at a 1° $\times$ 1.25° horizontal resolution (Chin, personal communications, 2013). The data are processed such that daily values of dust, BC, and OC, smoothed over the entire day, are deposited onto the modeled snowpack every 7 days, to simulate weekly aerosol deposition events (see section A3 for more details). This

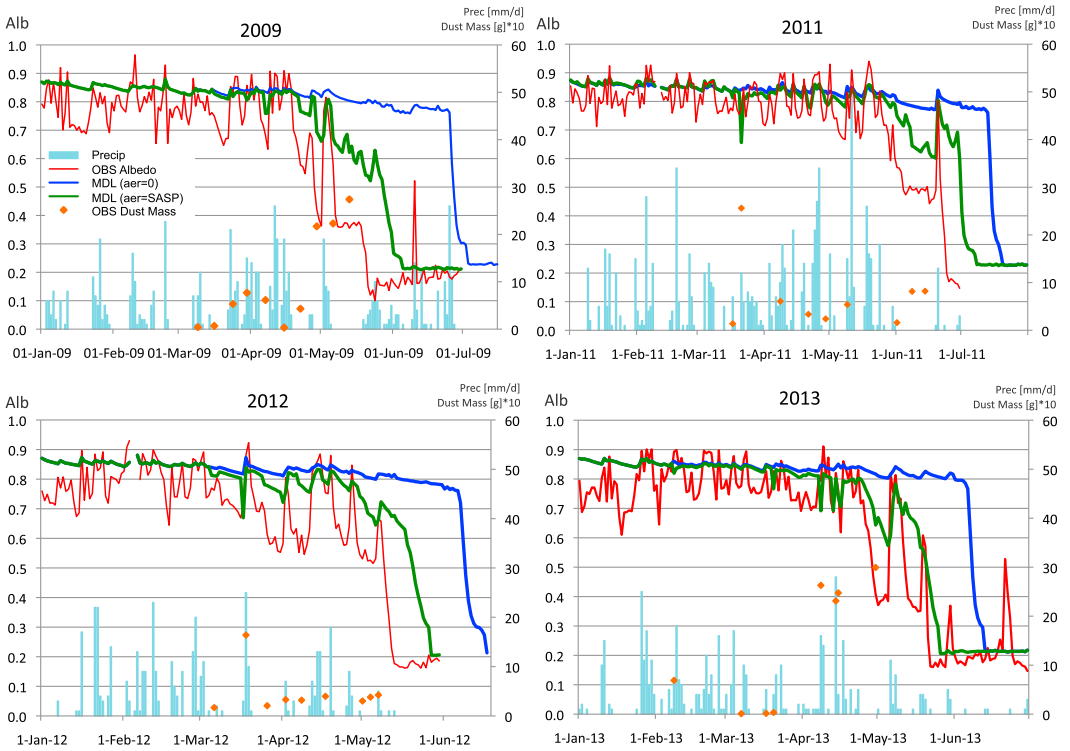

Figure 2. Observed and modeled albedo using SSiB-3/aer for four different years at the SASP site, along with precipitation [mm/day], dust events, and dust mass [g] × 10 (right vertical axis).

temporal interval is reasonable given observed springtime dust deposition events over the WUS [e.g., *Painter et al.*, 2012].

Snow Data Assimilation System (SNODAS) SWE reanalysis data available from the *National Operational Hydrologic Remote Sensing Center* [2004] (http://nsidc.org/data/docs/noaa/g02158_snodas_snow_cover_model/) are used for coupled model validation. SNODAS is a modeling and data assimilation system developed by the National Operational Hydrologic Remote Sensing Center that includes procedures to assimilate satellite-derived, airborne, and ground-based observations of snow-covered area and Snow Water Equivalent (SWE).

4. Results Analysis and Discussion

4.1. Offline Simulations

4.1.1. Snow Albedo

The performance of the new SSiB-3/aer is first evaluated by comparing the point-based offline simulations from the AER and NOAER scenarios to in situ observations for the SASP location. Figure 2 shows simulated and observed albedo for each of the 4 years, along with precipitation and dust-on-snow events for reference. The modeled albedo has an average bias over Jan–Jul for the 4 years of 0.08 and 0.16 and RMSE of 0.14 and 0.25, for AER and NOAER, respectively. During the accumulation period (defined as 1 January to 15 April), both AER and NOAER simulations behave similarly and are consistent with observations, albedo decreasing mostly due to snow aging during periods of no fresh snowfall, and increasing with new snow, dust in snow having little impact on albedo. The AER and NOAER simulations start to diverge from one another during the ablation period, from 15 April to snow-all-gone (SAG) date. The NOAER simulation is unable to correctly reproduce albedo evolution during the melting season, remaining too large throughout most of that time. On the other hand, the AER simulated albedo matches observations more closely, responding both to melting and to dust-on-snow deposition events. The difference between AER and NOAER simulations highlights the importance of considering aerosols in snow in model simulations, as the dust in the AER simulation lowers albedo significantly through both the direct and two indirect effects, and demonstrates that snow aging processes alone cannot explain the observed albedo reduction during the melting season.

Table 2. Statistics for SSiB-3/aer Model Runs (AER and NOAER) With Respect to In Situ Observations

	RMSE obs-AER	RMSE obs-NOAER	Correl Coeff obs-AER	Correl Coeff obs-NOAER	AER-OBS Bias	NOAER-OBS Bias	OBS stdev	AER stdev	NOAER stdev
Albedo									
2009	0.15	0.32	0.899	0.565	0.09	0.22	0.27	0.23	0.08
2011	0.13	0.18	0.857	0.83	0.07	0.10	0.17	0.21	0.16
2012	0.16	0.25	0.850	0.88	0.11	0.18	0.22	0.15	0.02
2013	0.11	0.24	0.927	0.66	0.06	0.14	0.25	0.25	0.20
Ave	0.14	0.25	0.88	0.73	0.08	0.16	0.23	0.21	0.12
Snow depth [m]									
2009	0.26	0.59	0.964	0.85	0.16	0.39	0.76	0.74	0.46
2011	0.26	0.37	0.963	0.881	0.15	0.18	0.47	0.39	0.35
2012	0.27	0.39	0.820	0.62	0.05	0.18	0.39	0.42	0.29
2013	0.12	0.35	0.983	0.874	0.03	0.09	0.37[a]	0.29[a]	0.25[a]
Ave	0.23	0.43	0.93	0.81	0.10	0.21	0.50	0.46	0.34
SWE [mm]									
2009	48.36	48.88	0.97	0.97	−7.84[a]	15.51[a]	126.29[b]	159.18[a]	120.12[a]
2011	86.71	141.01	0.98	0.88	13.57	29.59	213.40[b]	195.90[a]	183.69[a]
2012	137.64	469.34	0.660	0.40	26.98	75.11	131.70[b]	134.45[a]	107.25[a]
2013	38.58	90.91	0.989	0.782	−21.09	−1.28	129.08[b]	100.11[a]	108.11[a]
Ave	77.82	187.54	0.90	0.76	2.91	29.73	150.12	147.41	129.79
Aerosol mass [kg/m^2]									
Top layer 2013	1.00E−03		0.803						

[a]Calculation does not include 0 SWE values (i.e., only snow present in obs values).
[b]Small sample size [e.g., = 11 (2009)].

The external forcing due to deposition of dust and other aerosols to the snowpack must be taken into account through either specified, as did in this study, or interactive mode, as did in *Zhao et al*. [2014]. The improvement in the AER case is corroborated by the statistics in Table 2, which show that despite a slight positive systematic model bias in albedo, the AER simulation has an average RMSE (0.14) and bias (0.08) that are half of those of NOAER albedo (0.25 and 0.16, respectively), a higher temporal correlation (0.88 for AER case, 0.73 for NOAER), and a standard deviation that matched observations to within 91% (OBS stdev is 0.23, AER is 0.21, NOAER is 0.12).

4.1.2. Snow Depth

Simulated and observed snow depth is plotted in Figure 3, with the red line indicating the SAG date in observations. Simulated snow depth is consistent with the albedo results. During the accumulation period, there is little distinction between the clean (NOAER) and dirty (AER) snow simulations, both matching closely the observed snow depth magnitude and variability, capturing the gain and loss of snow mass due to new snowfall, compaction, and melt. However, during ablation, AER snow depth decreases at a pace closer to observations, while NOAER simulates a thicker snowpack, delaying the melting process and thus misrepresenting the length of the snow cover. As Table 3 shows, the clean snow simulation average snowpack duration is about a month longer (33 days) than that observed, whereas the dust-loaded snow cover duration is only about 14 days longer. While neither simulation matches observations exactly, the AER results have a smaller error (bias of 0.1; RMSE of 0.23) and better variability (temporal correlation of 0.93) compared to NOAER (bias of 0.21; RMSE of 0.43; temporal correlation of 0.81) over the simulated Jan–Jul period (Table 2).

4.1.3. Sensitivity Studies

Figure 4 shows how simulated albedo and snow depth might change if ω and/or dust mass are adjusted. A lower ω and doubled dust mass do not have a substantial impact until the ablation period, despite five dust events occurring prior to 15 April. However, during late spring and early summer, SSiB-3/aer becomes sensitive to such changes. Taking AER-st1 to be our control, where neither ω nor dust mass is modified, we observe that decreasing the ω only (by 0.2) (AER-st3) lowers albedo and snow depth more than a doubling of dust mass deposition (AER-st2). Altering both ω and dust mass (AER-st4) simulates albedo (Figure 4a) closest to observations, but snow depth (Figure 4b) is reduced too much during the ablation season compared to both observations and the other model scenarios, as the bias values in Figure 4c and Table 1b indicate: AER-st4 has the largest bias during the melting period (0.114) of all four sensitivity studies, whereas

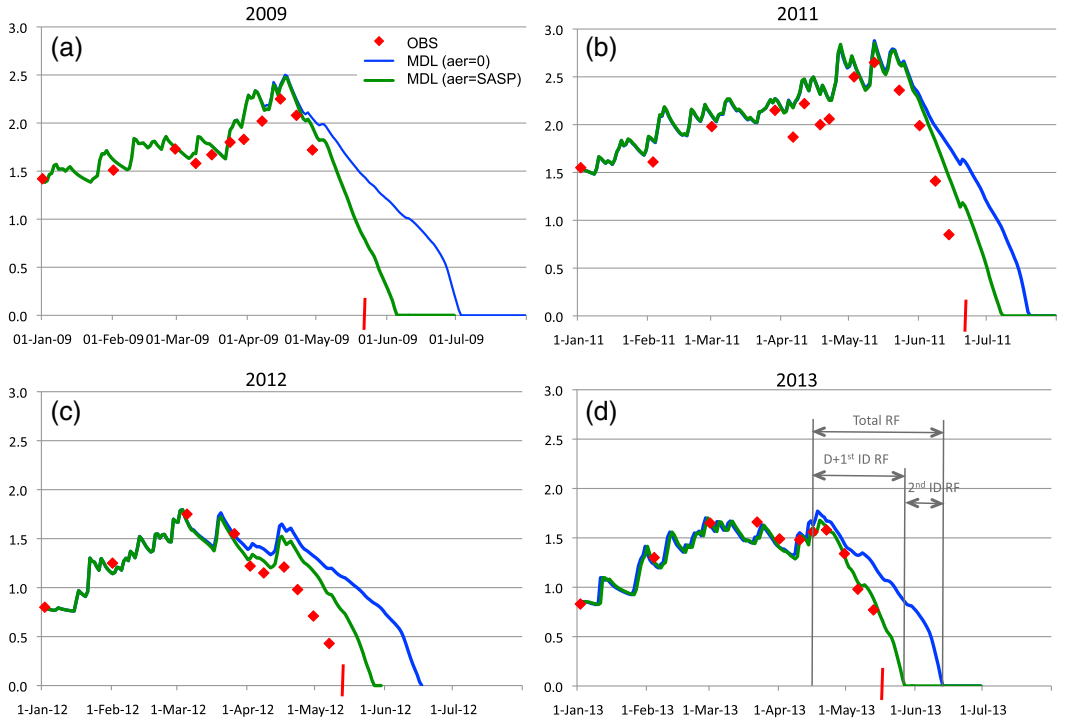

Figure 3. Observed and modeled snow depth [m] using SSiB-3/aer for four different years at the SASP site. Short red dash indicates observed snow-all-gone date. Grey lines and arrows in Figure 3d indicate periods over which various radiative forcings (RF) are calculated. D refers to "direct", 1st ID to "first indirect", and 2nd ID to "second indirect" RF.

AER-st3 has the lowest (0.045). Because AER-st3 results in smaller model bias, and recounting WUS dust is more absorptive than generic dust currently represented in SNICAR, we conduct the main simulations in this study by using adjusted ω values ($\omega - 0.2$).

4.1.4. Radiative Forcing

To quantify the impact dust in snow has on the surface energy budget, we calculate its radiative forcing (RF). RF is computed by taking the difference between net shortwave radiation (NSW) in the AER case and NSW in the NOAER case. *Total* RF of dust in snow, due to both the direct and two indirect effects introduced earlier, is calculated based on the NSW difference over the ablation period, here defined as 15 April to SAG in NOAER. In our simulations, total RF ranges from 32 to 80 W/m^2 for the 4 years, with an average of 54 W/m^2 additional energy absorbed at the surface (Table 4). These results are comparable to those found by previous observational studies at the SASP site, which found mean daily RF over the period 21 March to 21 June of 31–37 W/m^2 for 2005, and 56–64 W/m^2 for 2006, with a maxima of 80 W/m^2 [*Painter et al.*, 2007a]. *RF from the second indirect effect alone*, representing the additional amount of solar radiation absorbed at the surface due to earlier exposure of darker underlying layer, is the NSW difference over the period from SAG in AER case to SAG in NOAER scenario. We find a mean modeled RF over this interval of 118 W/m^2, with a range of 78 to 142 W/m^2 (Table 4). For clarity, the periods selected for RF calculations for the various effects are indicated visually in Figure 3d. The values in this study are within the range found by previous studies at the SASP site.

Table 3. Observed and Modeled (MDL) Snow-All-Gone (SAG) Dates and Corresponding Differences

Year	Observed SAG	AER MDL SAG	Obs-AER SAG Difference	NOAER MDL SAG	OBS-NOAER SAG Difference	NOAER-AER SAG Difference
2009	22 May	5 June	14 days	3 July	42 days	28
2011	22 June	9 July	17 days	20 July	29 days	12
2012	12 May	27 May	15 days	17 June	36 days	21
2013	18 May	27 May	9 days	13 June	26 days	17
Ave			13.75		33.25	19.5

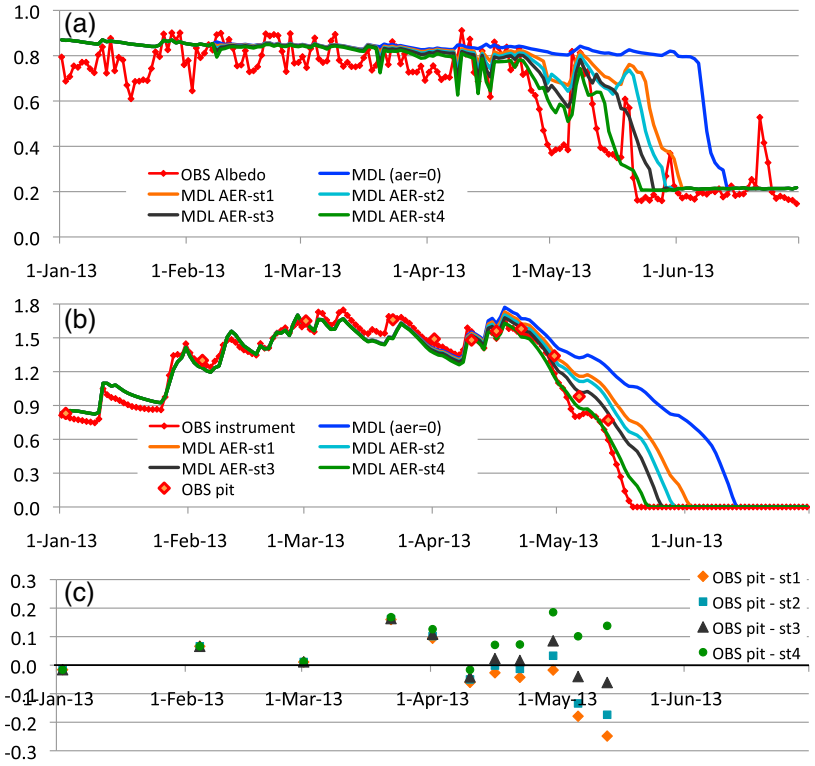

Figure 4. Modeled (a) albedo and (b) snow depth [m] for sensitivity studies described in Table 1b, along with observations (year 2013), and (c) sensitivity studies snow depth biases [m] with respect to observations (year 2013).

Painter et al. [2007a] calculated the 2nd, and indirect RF to be 147±8 W/m^2 at the SASP site for 2006, while *Skiles et al.* [2012] found 2nd indirect RF values over the period SAG observed to SAG in clean snow simulation (using a snow model only) of 136 W/m^2 in 2005 and 150 W/m^2 in 2006. Our model results, supported by previous observational studies, indicate that the influence of dust in snow at this location is substantial, with implications to the snowpack state as discussed above, and ultimately to runoff and water resources.

4.1.5. Snow Aging

We also validate the model's ability to simulate snow aging. Snow grain size evolution matters both during the accumulation period and perhaps more importantly during the melting season, when it enhances the effects of impurities in snow. Figure 5 presents stratigraphy of snow particle radius observed at the SASP location for the year 2011, along with modeled effective snow grain size averaged over the 4 years simulated. Because observed r_e is recorded every 2 cm vertically, while modeled snow is divided into only three layers, it is difficult to do a direct comparison. However, Figure 5 suggests the model is able to capture the main features of how r_e changes with depth. SSiB-3/aer generates the largest snow grains in the middle modeled layer, between 2 and 22 cm from the snow surface, which is consistent with observations at the SASP sites, where the largest

Table 4. Modeled Radiative Forcing, RF [W/m^2], Defined as AER_NSW–NOAER_NSW

Year	MDL RF [W/m^2] 15 Apr to NOAER SAG[a] (All Effects)	MDL RF [W/m^2] AER SAG to NOAER SAG[b] (Second Indirect Effect)
2009	70	120
2011	32	78
2012	58	130
2013	80	142
Ave	54	118

[a]15 April to NOAER SAG represents total RF from both direct and two indirect effects of dust in snow.
[b]AER SAG to NOAER SAG indicates the second indirect effect of dust in snow, the extra solar radiation absorbed by darker substrate/soil in the absence of snow (which would not be absorbed had dust not be present in snow, and snow had not melted sooner).

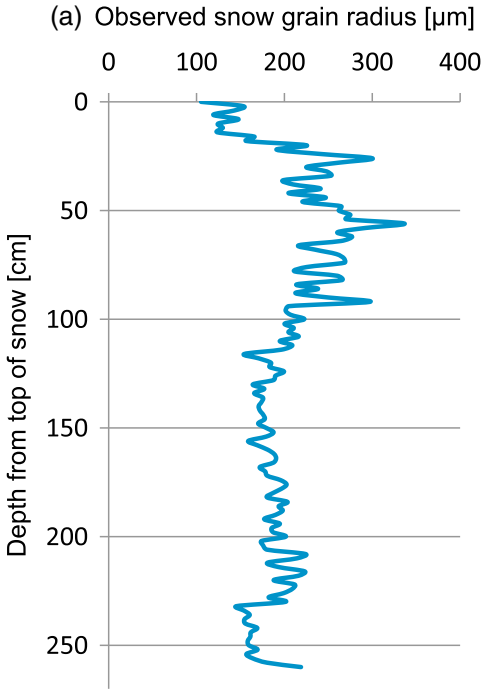

(b) Modeled effective snow grain radius [μm]

	Max r_e	Ave r_e
Top (0-2 cm)	216	95
Middle (2-22 cm)	470	320
Bottom (below 22 cm)	260	173

Figure 5. (a) Observed snow grain radius [μm] at SASP for year 2011 (average over following dates 12 Apr, 10 May, 12 May, 15 May, 10 Jun, and 16 Jun), and (b) modeled effective snow grain radius, r_e [μm], averaged over 4 years, for each model snow layer.

snow grains are found just below the top layer (Figure 5). This observation is corroborated by other field studies [e.g., *Painter et al*., 2007b].

4.1.6. Mass of Dust in Snow

The magnitude of the impact of impurities in snow depends on their location within the snowpack. Figure 6 shows how the mass of dust in each model snow layer changes over time during the 2013 spring season, along with precipitation and runoff for reference. Both the timing and magnitude of simulated dust mass in the top 2 cm of snow compare well to observed mass in the top 3 cm at the SASP site, with a temporal correlation of 0.8 and RMSE of 1.0E−03 (Table 2). Dust mass budget in SSiB-3/aer responds to precipitation events, which tend to reduce dust amount in top layer and increase mass in the middle and bottom layers. SSiB/aer also responds well to dust deposition events, increasing dust mass in the top layer, unless it happens to be a strong wet dust deposition event, in which case dust layers are quickly buried and placed in the layers below. These processes are in agreement with observations at this site [*Painter et al*., 2007a; *Skiles et al*., 2012]. Dust mass in the top layer also increases when there is compaction, melting, and little-to-no new snowfall, for example, during 30 April to 6 May (arrows in Figure 6). This occurs because the top snow layer itself is adjusted. In this case the top snow layer first decreases in depth due to compaction and melt, but is adjusted before the new time step by receiving some of the middle snow layers, and therefore aerosol mass, to be equal to 2 cm in thickness as intended (see sections A1 and A2 in Appendix A for more details on how snow layers and aerosol mass are adjusted). This means the top snow layer aerosol content increases since it receives some of the aerosol mass from the middle layer. As seen in Figure 6, during this period (30 April to 6 May) dust mass increases in the top layer while decreasing in the middle and bottom layers; the bottom layer is also losing dust and snow mass through runoff. The model tends to keep the dust in the top part of the snowpack as it is starting to melt, in agreement with previous field studies [e.g., *Conway et al*., 1996; *Painter et al*., 2007b].

The newly enhanced model generally captures the aerosol/snow physical processes. This point-based, offline study leads to the question of what is the impact of aerosols in snow on snowpack albedo, duration, and consequently runoff and overall hydrologic cycle, on a larger, regional scale such as WUS. Having SSiB-3/aer implemented in a regional climate model (WRF/SSiB-3/aer), as described earlier, allows us to investigate this question.

4.2. RCM Simulation

Using the RCM modeling framework, we examine (1) the improvement of the new model (WRF/SSiB-3/aer) with respect to the previous version (WRF/SSiB-3/orig), thus highlighting the importance of properly simulated snow processes, as well as (2) the impact of impurities in snow on the regional snowpack. Preliminary test results based on a 1-year simulation are presented in this section.

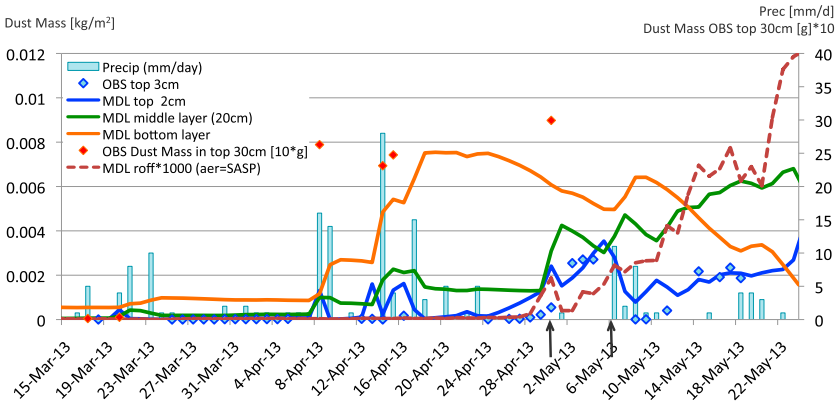

Figure 6. Observed dust mass in top 30 cm [g × 10] (right axis) and modeled dust mass [kg/m^2] (left axis) at SASP for year 2013, along with precipitation [mm/day] and modeled runoff [mm/day] for AER simulation (right axis).

Figure 7 shows the 2009 March–April–May (MAM) average SWE simulated with both the pre-modified (WRF/SSiB-3/orig) and improved (WRF/SSiB-3/aer) versions, and compared to SNODAS reanalysis. The newly enhanced RCM does well in capturing the main features of the SWE spatial distribution over WUS, especially over high topography such as the Sierra Nevada, Cascade, and Rocky mountain ranges, despite a negative bias in average magnitude of −17 mm. WRF/SSiB-3/aer reduces the bias with respect to SWE reanalysis by more than half compared to WRF/SSiB-3/orig, underlining the added value of including snow aging and vertically resolved snow radiative transfer explicitly in the model. WRF/SSiB-3/orig, in which vertically resolved radiative transfer and the effects of snow grain size and aerosols on the albedo were ignored, melts snow too soon, leading to an underestimated snowpack during springtime. Overall, the new model (WRF/SSiB-3/aer) simulates a higher SWE than the pre-modified version (WRF/SSiB-3/orig), resulting in a more realistic snow spatial distribution as shown in Figure 7. This is due to snow albedo in WRF/SSiB-3/aer being larger than in WRF/SSiB-3/orig during the accumulation period or when and where there is little-to-no aerosol deposition. In WRF/SSiB-3/orig, snow albedo is empirically set to 0.85 (in VIS) and reduced by 60% during melt (as discussed in section 2.1). In WRF/SSiB-3/aer, fresh snow has a small snow grain size (set to 54 μm), which causes a high snow albedo. Also recall that snow albedo is scaled by snow cover fraction, which is a function of snow depth, and will therefore be different in the original and modified WRF due to snow-albedo feedbacks.

Of great importance is understanding how aerosols in snow affect the snowpack regionally in the springtime. Figure 8 shows changes in modeled surface albedo, NSW radiation, skin temperature, and SWE between wrf_AER (aerosol-loaded snow) and wrf_NOAER (clean snow) simulations for MAM 2009. The inserted statistics in each panel represent the wrf_AER-wrf_NOARE average difference for albedo, NSW, skin temperature, and

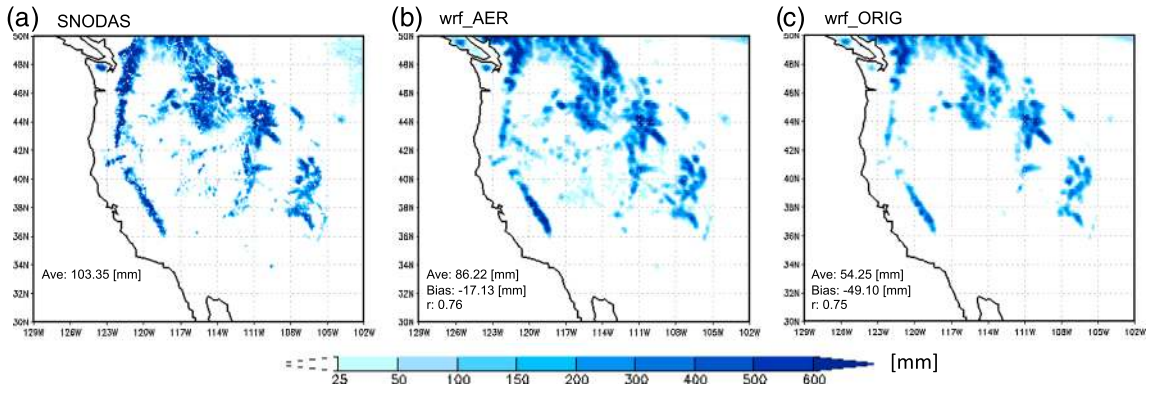

Figure 7. Snow water equivalent (SWE) [mm] for MAM 2009 in (a) SNODAS reanalysis product and modeled simulations with (b) WRF/SSiB-3/aer and (c) WRF-SSiB-3/orig RCMs. Statistics (average, bias, and spatial correlation with respect to reanalysis) for each data set are included in the bottom left corner of each panel.

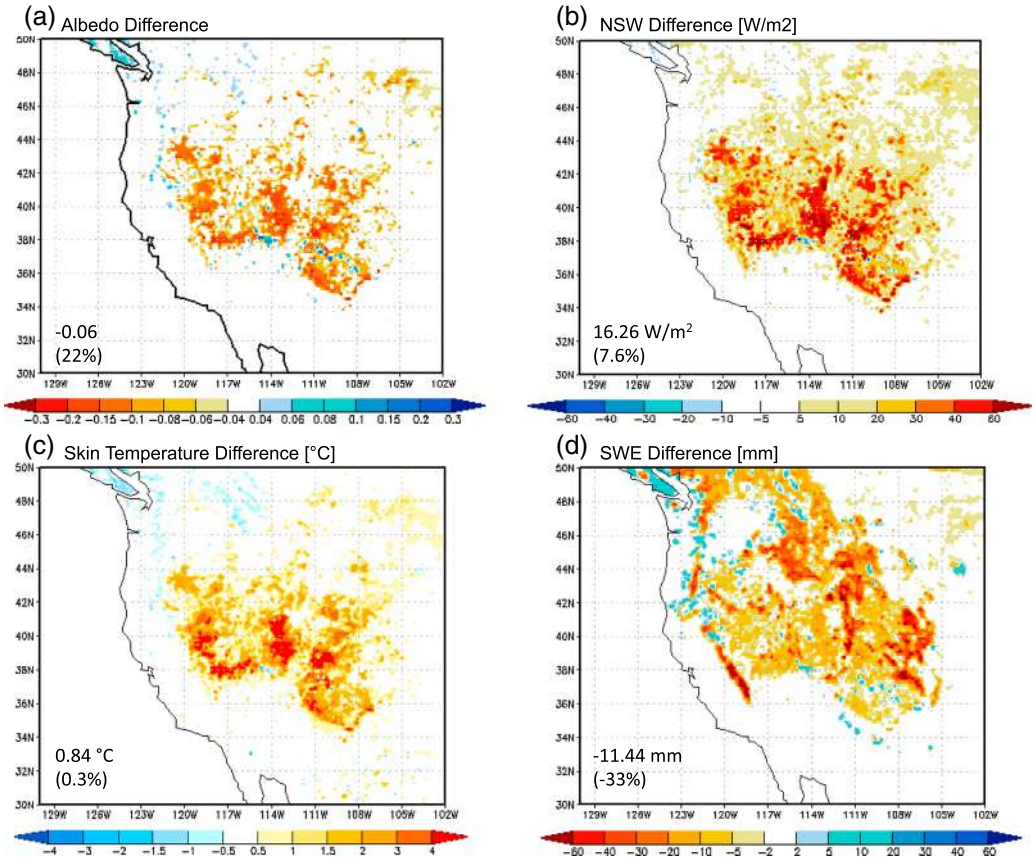

Figure 8. MAM 2009 difference in modeled (a) albedo, (b) net shortwave (NSW) radiation [W/m^2], (c) skin temperature [°C], and (d) SWE [mm] between wrf_AER and wrf_NOAER simulations using WRF/SSiB/aer. Statistics listed in each panel refer to area averages during MAM over 30–50°N, 129°W to 102°W, wherever difference for albedo, NSW, skin temperature, and SWE are greater than 0.02, 5 W/m^2, 0.2°C, and 1 mm, respectively, with the percent change in parentheses.

SWE over the domain 30–50°N, 129°W to 102°W during the MAM period, wherever this difference is greater than 0.02, 5 W/m^2, 0.2°C, and 1 mm, respectively. Percent change is also indicated in parentheses. There is a clear reduction in surface albedo when dust, BC, and OC are present in the simulated snow, by as much as 0.3 and an average of about 6% during MAM, a 22% change (Figure 8a). The larger changes are over the southern parts of WUS, in particular over the Southern Rockies and the intermontane Great Basin area. These regions correspond to significant surface dust deposition (Figure 9) in the GOCART forcing data set, which is in agreement with satellite-based observations of dust emission source areas [e.g., *Ginoux et al*., 2012]. Because surface albedo is lowered in the presence of aerosols in snow, NSW radiation increases, leading to an average radiative forcing of 16 W/m^2 (7.6% change) over the MAM period (Figure 8b) (again, this is averaged wherever RF difference is greater than 5 W/m^2, and over the domain 30–50°N, 129°W to 102°W as detailed above). This forcing causes a MAM average increase in skin temperature of 0.84°C (Figure 8c) over the specified domain and thus an overall decline in springtime SWE of about 11 mm, a −33% change (Figure 8d), with higher SWE reductions over mountainous, higher elevation areas (Figure 10b) where SWE is relatively larger.

The change in skin temperature, TSK, (ΔTSK) (Figure 8c) due to the presence of aerosols in snow varies in magnitude across the domain. Several studies suggest an elevation dependency of temperature change in response to climate drivers, although there is a disagreement as to whether warming rates increase or decrease with elevation (see *Rangwala and Miller* [2012], for a literature review). When plotted against topography height, our simulations do show a ΔTSK elevation dependency (Figure 11a). The largest ΔTSK over the MAM period occurs at relatively high elevations, between 1400 and 2400 m (Figures 11a and 11c) and above 3200 m, ranging 0.58°C to 0.92°C. At even higher elevations, 2400 to 3200 m, ΔTSK is still noteworthy though not as large,

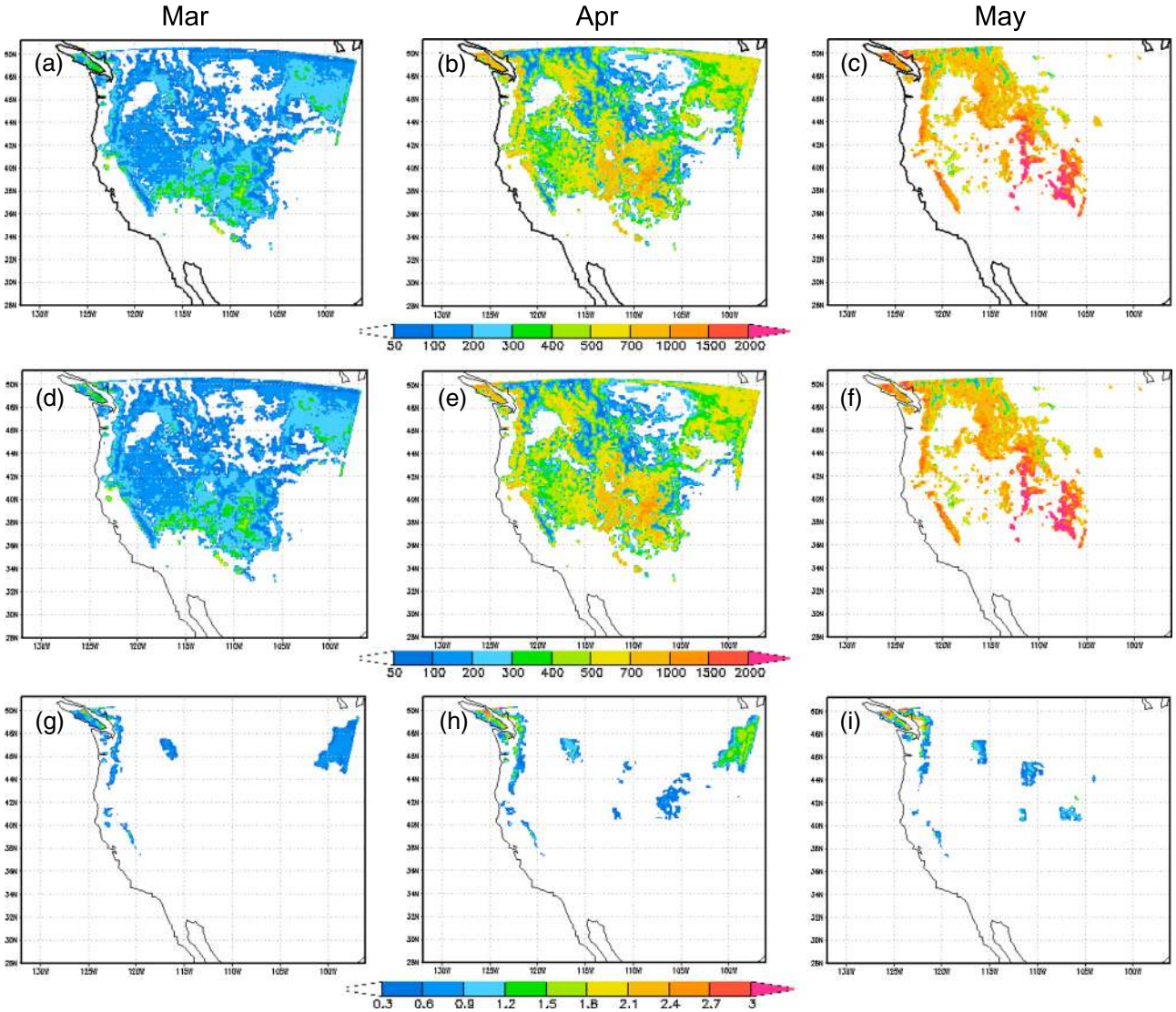

Figure 9. Spatial distribution for (left) Mar, (center) Apr, and (right) May of (a–c) total aerosol mass (dust + BC + OC) in top model snow layer; (d–f) dust mass only in top model snow layer; and (g–i) BC/OC mass only in top model snow. Units of mg/m^2. Note the different color bar for BC/OC plots (Figures 9g–9i) from the rest. (1 mm SWE mask is applied to all panels.)

ranging 0.35°C to 0.46°C. This relatively smaller ΔTSK at the higher elevations (2400–3200 m) might be explained by the difference in vegetation types found at these various elevations (in the model). Vegetation type in this elevation band is mostly needle-leaf evergreens (Figure 10a), whereas the 1400–2400 m band has shrubs with bare soil and/or dwarf tree with ground cover (Figure 11b). This suggests the taller vegetation (evergreens) contributes to moderate and suppress the temperature increase caused by the presence of aerosols in snow. The analysis of ΔTSK in conjecture with elevation, vegetation type, and freezing line suggests that in general ΔTSK due to aerosols in snow increases with elevations, but the location of the freezing line and taller bigger vegetation such as evergreens, if present, tend to suppress this warming. The interplay between aerosols in snow, snow albedo, TSK, SWE, elevation, and vegetation type require further study and will be addressed in a future paper.

It is important to note a few key shortcomings in using an offline surface aerosol deposition data set such as GOCART, as it may affect estimates of impact of aerosols in snow. Because the model used to provide the GOCART data is a global model, it has a relatively coarse spatial resolution (here 1° × 1.25°), which might cause it to miss the spatial and temporal variability of aerosol deposition on mountain snow, primarily due to the smoothing of high complex terrain, likely causing an underestimation of impacts of aerosols in snow.

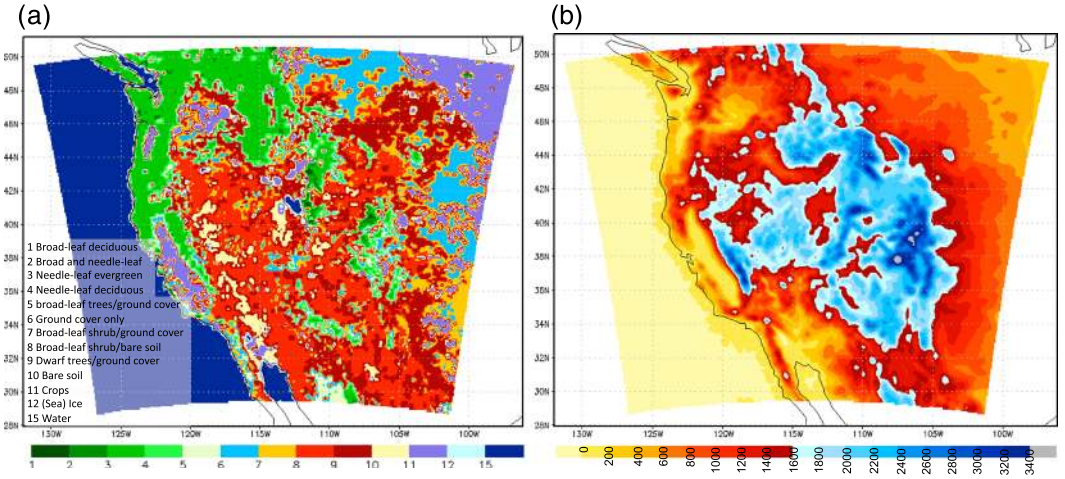

Figure 10. WRF/SSiB-3/aer (a) vegetation type; (b) elevation [m].

In addition, since GOCART was run separately from our RCM simulations, there is a discrepancy between timing of aerosol surface deposition and snowfall/snow accumulation. Based on the method of inputting the GOCART light-absorbing impurities in the RCM snow (section 3.2.2), the deposition onto the snowpack is done rather evenly through time (once every seventh day), and not synchronous with snow or rainfall events, which deposit aerosols through wet atmospheric removal. This mismatch implies some potential error in the vertical profile of aerosol concentrations in the snowpack. However, by adjusting the mass of aerosols in each snow layer when there is snowfall (including the top layer), our model accounts for the redistribution of aerosols in snow with new precipitation, even if the snowfall event may not match exactly

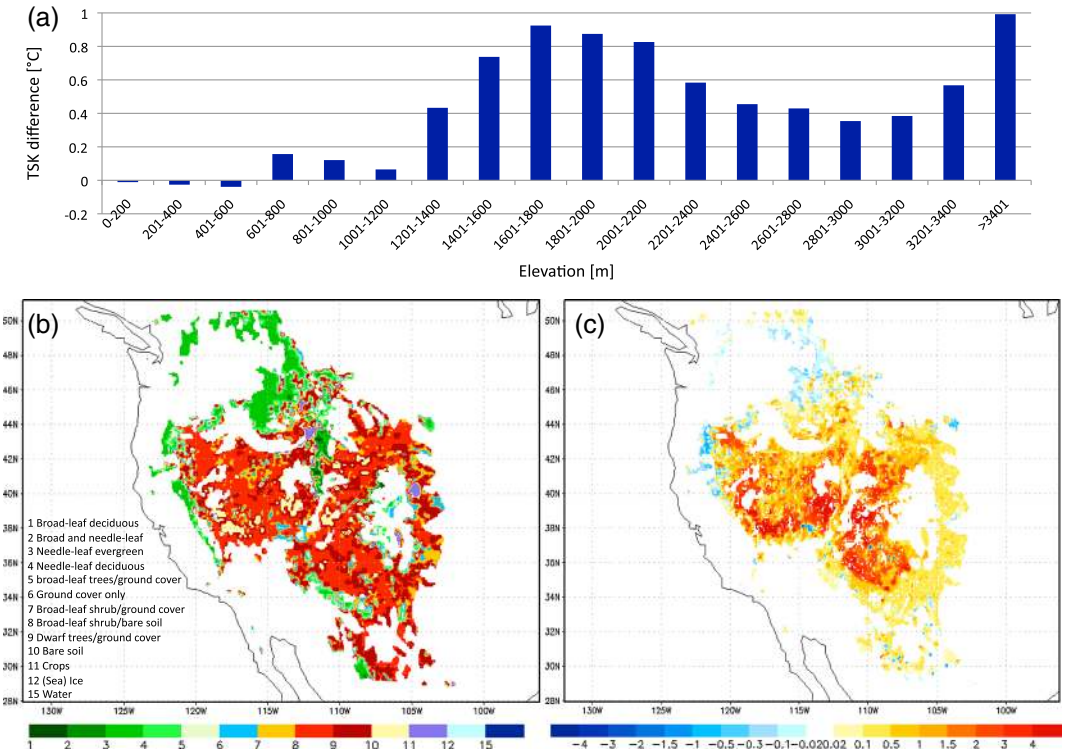

Figure 11. (a) wrf_AER-wrf_NOAER skin temperature (TSK) difference [°C] during MAM 2009 (averaged over a given elevation band) with respect to elevation [m]; (b) vegetation category for elevation band 1400–2400 m; and (c) wrf_AER-wrf_NOAER TSK difference [°C] during MAM 2009 wherever elevation is 1400–2400 m.

with a potential wet deposition aerosol event. While coupled online simulation framework is desirable (e.g., use of WRF with "chemistry" component "on"), this is a challenging subject and heavily dependent on the proper specification of dust source emission. There is still much uncertainty in processes controlling dust emission characteristics, including dust size distribution [e.g., *Reid et al*., 2003] and spatial variability. Furthermore, there has been limited use and evaluation of WRF-Chem ability to emit, transport, and deposit dust across WUS region, leading to uncertainties. While we acknowledge the potential of WRF-Chem to be used in coupled mode with the framework presented here in order to improve certain aspects of the simulation, because of the existing uncertainties, we feel that use of GOCART data as the surface aerosol forcing data in our WRF/SSiB-3/aer simulations is a reasonable method.

5. Conclusions

We improved snow processes in the Simplified Simple Biosphere (SSiB-3) land surface model coupled with the Weather Research and Forecasting/Advanced Research WRF (WRF-ARW) regional climate model (RCM), by incorporating the snow-aging, interactive snow-aerosol radiative transfer SNICAR model. The original snow albedo in WRF/SSiB-3 is replaced by the physically based albedo provided by SNICAR, while absorbed radiation within the snowpack calculated by SNICAR is used in surface energy and water balance in SSiB-3. The land surface model is further modified to account for deposition, movement, and removal by meltwater of aerosols in the snowpack. The result is one of few regional models that allow for realistic simulation and investigation of how changes to snow albedo can affect the water and energy balance, snowcover and snowmelt, and climate on a regional scale, including changes due to impurities in snow.

Offline validation of the new model shows it can realistically reproduce snowpack properties, especially in the spring when snow begins to melt and aerosols in snow have a significant impact. The aerosol-loaded scenario simulates snow albedo and snow depth that match observations better than the clean snow case. Bias is reduced by about 50% in the aerosol-loaded scenario, and correlation is improved relative to clean snow. In the case when no impurities are present in snow, snow cover duration is overestimated by about a month, while the dirty snow simulation reproduces snow cover duration closer to that observed, within about 13 days. The point-based simulation for the location in the San Juan Mountains in the Southern Rockies of the WUS suggests an average dust-in-snow radiative forcing of 54 W/m^2 during MAM for the 4 years simulated. On a regional scale, the newly improved RCM produces a springtime radiative forcing over WUS of 16 W/m^2, a consequence of surface albedo being reduced by about 6% in the presence of impurities in snow. This forcing causes the skin temperature to increase by 0.84°C and leads to a WUS snowpack loss of about 11 mm averaged over the four simulated MAM seasons. WRF/SSiB-3/aer model results suggest an overall elevation dependency for change in TSK for the WUS region, with higher elevations (1400–2400 m) experiencing larger increase in TSK (0.58–0.92°C) due to aerosols in snow, although certain vegetation type and freezing line location can suppress such effects.

The RCM results are a preliminary look at the impact of dust, BC, and OC in snow when a regional climate model with physically based, comprehensive snow-aerosol interactions is used. One of the benefits of this model is that it could be used over any region of the world, at varying regional scales and spatial resolutions, and its output could be used in hydrologic models for various local and regional applications. Additionally, because the model considers both snow aging and aerosols in snow explicitly, it can be employed for simulations under a changing climate, including effects such as warmer temperatures affecting grain size evolution, increased dust emission and deposition due to increased drought-like conditions, and increased BC emissions.

The work presented here is a major step toward improving modeling of snow and aerosols-in-snow effects on a regional scale; however, some uncertainties remain. The use of offline GOCART aerosol deposition in snow causes a mismatch between the timing of aerosol deposition on snow, snowfall, and wet deposition events. This can lead to uncertainties in vertical distribution of aerosols within the snowpack. Employing an atmospheric chemistry model coupled to the RCM framework presented here is desirable to account for such discrepancies. In addition, the modeled vertical profile of aerosols concentration in snow is also sensitive to the scavenging parameter, k, which in turns affects the magnitude of RF of aerosols in snow, as shown in a recent study by *Qian et al*. [2014]. They found that a 10-time increase in default value of k ($0.02 \rightarrow 2.0$) leads to a decrease in aerosol concentration in snow that was consistent with a decrease in

RF of up to 2–3 W/m^2 over WUS (10-year April mean). However, the k values used in the work presented here, taken from *Conway et al.* [1996], are in general agreement with more recent work by *Doherty et al.* [2013]. Based on current knowledge about the scavenging of aerosols in snow by meltwater, we do not expect k to vary much, thus having minimal impact on estimated RF in this study.

Appendix A

A1. Snow Layers in SSiB-3

The SSiB-3 land surface model can have up to three snow layers, depending on the total thickness of the snowpack. If snow depth is less than the critical snow depth value, currently defined as 7 cm, there is only one snow layer. If snow accumulation surpasses 7 cm, the snowpack is divided into three layers, according to the following method: (i) if total snowpack depth is between 7 and 8 cm, the top and middle snow layers are each set to 2 cm, and the bottom to the remaining snow depth; (ii) if total snowpack depth is between 8 and 62 cm, the top layer is set to 2 cm, middle to 1/3 and bottom to 2/3 of the remaining depth; and (iii) if the snowpack is thicker than 62 cm, top snow layer is set to 2 cm, middle to 20 cm, and bottom to the remainder.

During a given model time step, each snow layer may change due to new snowfall, compaction, and melt. At the end of that time step, the snow layers are adjusted such that the top layer equals 2 cm. For example, if there is new snowfall during a given time step, the top snow layer will gain snow, thus increasing in depth. However, this will cause some snow compaction to occur, perhaps causing the top layer depth to fall below 2 cm. Before the end of the time step, the model will adjust the snow layers, taking some snow from the middle layer and placing it in the top layer, such that the top can be 2 cm; this causes the middle and bottom layers to also be adjusted accordingly. For further details about the method of layering snow in SSiB-3, please refer to *Sun et al.* [1999].

A2. Tracking Aerosols Mass Within Model Snowpack

With the introduction of aerosols in snow in the modeling framework (both SSiB-3 and WRF/SSiB-3), we had to account for how aerosol mass changes within a given snow layer depending on how the snowpack changes. When total snow depth goes below 7 cm, the three snow layers are combined into a single layer. Accordingly, aerosol mass corresponding to each of those layers will be combined into a single mass value, representative of the single snow layer. On the other hand, when the snowpack grows to above 7 cm threshold, it will be divided into three snow layers as described in the previous section. Total aerosol mass in this case is also divided into three layers. For examples, aerosol mass in the top layer (aer_mass_3) is set to the ratio (R_1) of the bottom snow layer thickness (dz_1) to total snow thickness, times total aerosol mass (aer_mass_total), whereas the bottom layer aerosol mass (aer_mass_1) is set to the ratio (R_3) of top snow layer thickness (dz_3) to total snow thickness, times total aerosol mass (aer_mass_total):

$$R_i = dz_i/dz_{\text{total}}, \quad \text{for } i = 1, 2, 3$$
$$\text{aer\_mass}_1 = R_3 * \text{aer\_mass\_total}$$
$$\text{aer\_mass}_2 = R_2 * \text{aer\_mass\_total}$$
$$\text{aer\_mass}_3 = R_1 * \text{aer\_mass\_total}$$

where $i = 1$ is the bottom layer, $i = 2$ is the middle layer, and $i = 3$ is the top snow layer. This method is used because it has been found by previous studies [e.g., *Conway et al.*, 1996; *Flanner et al.*, 2007] that aerosols in snow tend to remain toward the top of the snowpack (even during melting) or in the layer they were originally deposited in. Splitting single aerosol mass (into the three corresponding layers) inversely proportional to how snow layer depth is defined allows us to keep the bulk of the aerosol mass toward the top of the pack.

During the ablation period, when there is meltwater in the snowpack, aerosols throughout the snow may be scavenged by this meltwater. The efficiency with which meltwater can move or remove aerosols depends on the type of aerosols present. Here we use species-dependent scavenging ratio derived from *Conway et al.* [1996] (see Table A1). If the snow is a single layer, runoff within the pack will remove aerosol mass altogether (amount depended on efficiency). On the other hand, if the snow is multi-layer, aerosol mass may be moved from a layer to the one below according to equation (6) in the main text.

Each of these snow layers themselves can change (during a given time step) due to new snowfall, compaction, and melting, as described in section A1. When this happens, aerosol mass is adjusted proportionally with

Table A1. Meltwater Scavenging Efficiency Coefficient *k* for Particles in Snow, Based on *Conway et al.* [1996]

Species	*k*
Hydrophilic black carbon	0.20
Hydrophobic black carbon	0.03
Hydrophilic organic carbon	0.20
Hydrophobic organic carbon	0.03
Dust species 1 (0.05–0.5 μm)	0.02
Dust species 2 (0.5–1.25 μm)	0.02
Dust species 3 (1.25–2.5 μm)	0.01
Dust species 2 (2.5–5 μm)	0.01

howmuch the snow layer depth itself has changed. For example, if the top snow layer decreases in depth within a given time step due to compaction and melt, it is adjusted before the new time step by receiving some of the middle snow layers, and therefore aerosol mass, to be equal to 2 cm in thickness (as explained in section A1). This means the top snow layer aerosol content also increases since it receives some of the aerosol mass from the middle layer.

A3. Processing GOCART Data for Input to WRF

For this work, the GOCART group provided monthly accumulations of these aerosols for 2009 at a 1° × 1.25° horizontal resolution (Chin, personal communications, 2013). In order for these data to be ingested by WRF/SSiB-3/aer, several steps have to be taken: (i) data are transformed to a regular 1° × 1° horizontal resolution; (ii) data are converted to needed units: dust from kg/box to kg/m^2, and BC and OC from mole/box to kg/m^2 using the following:

$$\text{dustMass}\left[\frac{\text{kg}}{\text{box}}\right]/\text{gridBoxArea}\left[\frac{\text{m}^2}{\text{box}}\right]=\text{dust}\left[{}^{\text{kg}}/_{\text{m}^2}\right]$$

$$\left(\text{BCmass}\left[\frac{\text{mole}}{\text{box}}\right]\times\text{molecularMass}\left[\frac{\text{g}}{\text{mol}}\right]\times\frac{1\text{kg}}{1000\text{g}}\right)/\text{gridBoxArea}\left[\frac{\text{m}^2}{\text{box}}\right]=\text{BC}\left[{}^{\text{kg}}/_{\text{m}^2}\right]$$

where a grid box area is provided in the data set, and molecular mass of BC is 12 g/mol; (iii) wet and dry deposition values are summed together to give total deposition; and (iv) WRF takes the accumulated monthly aerosol values and places them at the 15$^{\text{th}}$ of each month, then interpolates to a daily value. For this study, every seventh day value is used as input and deposited onto the modeled snowpack, smoothed over the entire day, to simulate weekly aerosol deposition events.

GOCART provides surface dust deposition amount in four bins: bin 1 is 0.1–1.0 μm, bin 2 is 1.0–1.8 μm, bin 3 is 1.8–3.0 μm, and bin 4 is 3–6 μm. A note should be made that SNICAR bin sizes, which are important when optical properties for a given dust grain is extracted for RT calculations, are slightly different: bin 1 is 0.05–0.5 μm, bin 2 is 0.5–1.25 μm, bin 3 is 1.25–2.5 μm, and bin 4 is 2.5–5.0 μm. In our study, we prescribe GOCART bin size 1 dust amount to correspond to SNICAR bin size 1 optical properties, GOCART bin 2 to SNICAR bin 2, GOCART bin 3 to SNICAR bin 3, and GOCART bin 4 to SNICAR bin 4. GOCART bin size 5 is not presently used. The discrepancy in bin sizes is small, and they match fairly closely considering how the bins line up on the log-normal dust size distribution found in WUS. We therefore do not anticipate this to have a large impact on our simulations.

Acknowledgments
We thank Mian Chin of NASA Goddard Space Flight Center and her group for providing the GOCART aerosol deposition data set for use in this study. Additional data used in this study are available from the corresponding author (oaidac@ucla.edu). This research was supported by NASA grant NNX10A097G, NSF grant AGS-1115506,, NSF grant AGS-1346813, and the UCLA Graduate Dissertation Year Fellowship. The WRF model simulations were conducted using NCAR supercomputing resources. Part of this work was performed at the Jet Propulsion Laboratory, California Institute of Technology under a contract with NASA.

References

Belnap, J., and D. A. Gillette (1998), Vulnerability of desert biological soil crusts to wind erosion: The influences of crust development, soil texture, and disturbance, *J. Arid Environ.*, *39*, 133–142, doi:10.1006/jare.1998.0388.

Belnap, J., R. L. Reynolds, M. C. Reheis, S. L. Phillips, F. E. Urban, and H. L. Goldstein (2009), Sediment losses and gains across a gradient of livestock grazing and plant invasion in a cool, semi-arid grassland, Colorado Plateau, USA, *Aeolian Res.*, *1*(1–2), 27–43, doi:10.1016/j.aeolia.2009.03.001.

Blackford, J. R. (2007), Sintering and microstructure of ice: A review, *J. Phys. D: Appl. Phys.*, *40*, R355–R385, doi:10.1088/0022-3727/40/21/R02.

Bond, T. C., E. Bhardwaj, R. Dong, R. Jogani, S. Jung, C. Roden, D. G. Streets, and N. M. Trautmann (2007), Historical emissions of black and organic carbon aerosol from energy-related combustion, 1850–2000, *Global Biogeochem. Cycles*, *21*, GB2018, doi:10.1029/2006GB002840.

Brun, E. (1989), Investigation of wet-snow metamorphism in respect of liquid-water content, *Ann. Glaciol.*, *13*, 22–26.

Budyko, M. I. (1969), The effect of solar radiation variations on the climate of the Earth, *Tellus*, *21*, 611–619, doi:10.1111/j.2153-3490.1969.tb00466.x.

Chin, M., R. B. Rood, S.-J. Lin, J.-F. Müller, and A. Thompson (2000), Atmospheric sulfur cycle simulated in the global model GOCART: Model description and global properties, *J. Geophys. Res.*, *105*(D20), 24,671–24,687, doi:10.1029/2000JD900384.

Chin, M., P. Ginoux, S. Kinne, O. Torres, B. Holben, B. N. Duncan, R. V. Martin, J. Logan, A. Higurashi, and T. Nakajima (2002), Tropospheric aerosol optical thickness from the GOCART model and comparisons with satellite and sun photometer measurements, *J. Atmos. Phys.*, *59*, 461–483, doi:10.1175/1520-0469(2002)059<0461:TAOTFT>2.0.CO;2.

Christensen, J. H., et al. (2007), Regional climate projections, in *Climate Change 2007: The Physical Science Basis. Contribution of Working Group I to the Fourth Assessment Report of the Intergovernmental Panel on Climate Change*, edited by S. Solomon et al., Cambridge Univ. Press, Cambridge, U. K., and New York.

Colbeck, S. C. (2001), Sintering of unequal grains, *J. Appl. Phys.*, *89*(8), 4612–4618, doi:10.1063/1.1356427.
Conway, H., A. Gades, and C. F. Raymond (1996), Albedo of dirty snow during conditions of melt, *Water Resour. Res.*, *32*(6), 1713–1718, doi:10.1029/96WR00712.
De Sales, F., and Y. Xue (2012), Dynamic downscaling of 22-year CFS winter seasonal forecasts with the UCLA-ETA regional climate model over the United States, *Clim. Dyn.*, *41*, 255–275, doi:10.1007/s00382-012-1567-x.
Doherty, S. J., T. C. Grenfell, S. Forsström, D. L. Hegg, R. E. Brandt, and S. G. Warren (2013), Observed vertical redistribution of black carbon and other insoluble light-absorbing particles in melting snow, *J. Geophys. Res. Atmos.*, *118*, 5553–5569, doi:10.1002/jgrd.50235.
Flanner, M. G., and C. S. Zender (2005), Snowpack radiative heating: Influence on Tibetan Plateau climate, *Geophys. Res. Lett.*, *32*, L06501, doi:10.1029/2004GL022076.
Flanner, M. G., and C. S. Zender (2006), Linking snowpack microphysics and albedo evolution, *J. Geophys. Res.*, *111*, D12208, doi:10.1029/2005JD006834.
Flanner, M. G., C. S. Zender, J. T. Randerson, and P. J. Rasch (2007), Present-day climate forcing and response from black carbon in snow, *J. Geophys. Res.*, *112*, D11202, doi:10.1029/2006JD008003.
Flanner, M. G., C. S. Zender, P. G. Hess, N. M. Mahowald, T. H. Painter, V. Ramanathan, and P. J. Rasch (2009), Springtime warming and reduced snow cover from carbonaceous particles, *Atmos. Chem. Phys.*, *9*, 2481–2497, doi:10.5194/acp-9-2481-2009.
Fukuzawa, T., and E. Akitaya (1993), Depth-hoar crystal growth in the surface layer under high temperature gradient, *Ann. Glaciol.*, *18*, 39–45.
Ghan, S. J., and T. Shippert (2006), Physically based global downscaling: Climate change projections for a full century, *J. Clim.*, *19*, 1589–1604, doi:10.1175/JCLI3701.1.
Ginoux, P., M. Chin, I. Tegen, J. M. Prospero, B. Holben, O. Dubovik, and S.-J. Lin (2001), Sources and distributions of dust aerosols simulated with the GOCART model, *J. Geophys. Res.*, *106*(D17), 20,255–20,273, doi:10.1029/2000JD000053.
Ginoux, P., J. M. Prospero, O. Torres, and M. Chin (2004), Long-term simulation of global dust distribution with GOCART model: Correlation with North Atlantic Oscillation, *Environ. Modell. Softw.*, *19*(2), 113–128.
Ginoux, P., J. M. Prospero, T. E. Gill, N. C. Hsu, and M. Zhao (2012), Global-scale attribution of anthropogenic and natural dust sources and their emission rates based on MODIS Deep Blue aerosol products, *Rev. Geophys.*, *50*, RG3005, doi:10.1029/2012RG000388.
Gleason, K. E., and A. W. Nolin (2013), New parameterization of the post-fire snow albedo effect, Abstract C43B-0681 presented at 2013 Fall Meeting, AGU, San Francisco, Calif., 9–13 Dec.
Hansen, J., and L. Nazarenko (2004), Soot climate forcing via snow and ice albedos, *Proc. Natl. Acad. Sci. U.S.A.*, *101*(2), 423–428, doi:10.1073/pnas.2237157100.
Hansen, J., et al. (2005), Efficacy of climate forcings, *J. Geophys. Res.*, *110*, D18104, doi:10.1029/2005JD005776.
Legagneux, L., A.-S. Taillandier, and F. Domine (2004), Grain growth theories and the isothermal evolution of the specific surface area of snow, *J. Appl. Phys.*, *95*(11), 6175–6184, doi:10.1063/1.1710718.
Leung, L. R., and Y. Qian (2003), The sensitivity of precipitation and snowpack simulations to model resolution via nesting in regions of complex terrain, *J. Hydrometeorol.*, *4*(6), 1025–1043, doi:10.1175/1525-7541(2003)004<1025:TSOPAS>2.0.CO;2.
Leung, L. R., Y. Qian, J. Han, and J. O. Roads (2003), Intercomparison of global reanalyses and regional simulations of cold season water budgets in the western United States, *J. Hydrometeorol.*, *4*(6), 1067–1087, doi:10.1175/1525-7541(2003)004<1067:IOGRAR>2.0.CO;2.
Li, J., G. S. Okin, S. M. Skiles, and T. H. Painter (2013), Relating variation of dust on snow to bare soil dynamics in the western United States, *Environ. Res. Lett.*, *8*, 044054, doi:10.1088/1748-9326/8/4/044054.
Liu, L. Y., X. Y. Li, P. J. Shi, S. Y. Goa, J. H. Wang, W. Q. Ta, Y. Song, M. X. Liu, Z. Wang, and B. L. Xiao (2007), Wind erodibility of major soils in the farming-pastoral ecotone of China, *J. Arid Environ.*, *68*, 611–623, doi:10.1016/j.jaridenv.2006.08.011.
Marbouty, D. (1980), An experimental study of the temperature-gradient metamorphism, *J. Glaciol.*, *26*(94), 303–312.
Ming, J., H. Cachier, C. Xiao, D. Qin, S. Kang, S. Hou, and J. Xu (2008), Black carbon record based on a shallow Himalayan ice core and its climatic implications, *Atmos. Chem. Phys.*, *8*, 1343–1352, doi:10.5194/acp-8-1343-2008.
National Operational Hydrologic Remote Sensing Center (2004), *Snow Data Assimilation System (SNODAS) Data Products at NSIDC*, [MAM 2009], Natl. Snow and Ice Data Cent., Boulder, Colo., doi:10.7265/N5TB14TC.
Neff, J. C., A. P. Ballantyne, G. L. Farmer, N. M. Mahowald, J. L. Conroy, C. C. Landry, J. T. Overpeck, T. H. Painter, C. R. Lawrence, and R. L. Reynolds (2008), Increasing eolian dust deposition in the western United States linked to human activity, *Nat. Geosci.*, *1*, 189–195, doi:10.1038/ngeo133.
Oleson, K. W., et al. (2010), Technical description of version 4.0 of the Community Land Model (CLM), *NCAR Tech. Note*. [Available at www.cesm.ucar.edu/models/ccsm4.0/clm/CLM4_Tech_Note.pdf.]
Painter, T. H., A. P. Barrett, C. C. Landry, J. C. Neff, M. P. Cassidy, C. R. Lawrence, K. E. McBride, and G. L. Farmer (2007a), Impact of disturbed desert soils on duration of mountain snow cover, *Geophys. Res. Lett.*, *34*, L12502, doi:10.1029/2007GL030284.
Painter, T. H., N. Molotch, M. Cassidy, M. Flanner, and K. Steffen (2007b), Contact spectroscopy for the determination of stratigraphy of snow grain size, *J. Glaciol.*, *53*(180), 121–127.
Painter, T. H., J. S. Deems, J. Belnap, A. F. Hamlet, C. C. Landry, and B. Udall (2010), Response of Colorado River runoff to dust radiative forcing in snow, *Proc. Natl. Acad. Sci. U.S.A.*, doi:10.1073/pnas.0913139107.
Painter, T. H., S. M. Skiles, J. S. Deems, A. C. Bryant, and C. C. Landry (2012), Dust radiative forcing in snow of the Upper Colorado River Basin: 1. A 6 year record of energy balance, radiation, and dust concentrations, *Water Resour. Res.*, *48*, W07521, doi:10.1029/2012WR011985.
Qian, Y., W. I. Gustafson Jr., L. R. Leung, and S. J. Ghan (2009), Effects of soot-induced snow albedo change on snowpack and hydrological cycle in western United States based on Weather Research and Forecasting chemistry and regional climate simulations, *J. Geophys. Res.*, *114*, D03108, doi:10.1029/2008JD011039.
Qian, Y., S. J. Ghan, and L. R. Leung (2010), Downscaling hydroclimatic changes over the Western US based on CAM subgrid scheme and WRF regional climate simulations, *Int. J. Climatol.*, *30*, 675–693, doi:10.1002/joc.1928.
Qian, Y., M. G. Flanner, L. R. Leung, and W. Wang (2011), Sensitivity studies on the impacts of Tibetan Plateau snowpack pollution on the Asian hydrological cycle and monsoon climate, *Atmos. Chem. Phys.*, *11*, 1929–1948, doi:10.5194/acp-11-1929-2011.
Qian, Y., H. Wang, R. Zhang, M. G. Flanner, and P. J. Rasch (2014), A sensitivity study on modeling black carbon in snow and its radiative forcing over the Arctic and Northern China, *Environ. Res. Lett.*, *9*(6), 064001, doi:10.1088/1748-9326/9/6/064001.
Qu, X., and A. Hall (2007), What controls the strength of snow-albedo feedback?, *J. Clim.*, *20*, 3971–3981, doi:10.1175/JCLI4186.1.
Rangwala, I., and J. R. Miller (2012), Climate change in mountains: A review of elevation-dependent warming and its potential causes, *Clim. Change*, *114*, 527–547, doi:10.1007/s10584-012-0419-3.
Rasmussen, R. M., et al. (2011), High-resolution coupled climate runoff simulations of seasonal snowfall over Colorado: A process study of current and warmer climate, *J. Clim.*, *24*, 3015–3048, doi:10.1175/2010JCLI3985.1.

Reid, J. S., et al. (2003), Comparison of size and morphological measurements of dust particles from Africa, *J. Geophys. Res.*, *108*, 8593, doi:10.1029/2002JD002485.

Rutter, N., et al. (2009), Evaluation of forest snow processes models (SnowMIP2), *J. Geophys. Res.*, *114*, D06111, doi:10.1029/2008JD011063.

Sellers, P. J., et al. (1996), A revised land surface parameterization (SiB2) for atmospheric GCMs. Part I: Model formulation, *J. Clim.*, *9*, 676–705, doi:10.1175/1520-0442(1996)009<0676:ARLSPF>2.0.CO;2.

Shamarock, W. C., J. B. Klemp, J. Dudhia, D. O. Gill, D. M. Barker, M. G. Duda, X.-Y. Huang, W. Wang, and J. G. Powers (2008), A description of the advanced research WRF version 3, *NCAR Tech. Note*. [Available at www.mmm.ucar.edu/wrf/users/docs/arw_v3.pdf.]

Shrestha, M., L. Wang, T. Koike, Y. Xue, and Y. Hirabayashi (2012), Modeling the spatial distribution of snow cover in the Dudhkoshi region of the Nepal Himalaya, *J. Hydrometeorol.*, *13*, 204–222, doi:10.1175/JHM-D-10-05027.1.

Skiles, S. M. (2014), *Dust and Black Carbon Radiative Forcing Controls on Snowmelt in the Colorado River Basin (Doctoral Dissertation)*, Univ. of California-Los Angeles, Los Angeles, Publisher: ProQuest, document ID# 3637640.

Skiles, S. M., T. H. Painter, J. S. Deems, A. C. Bryant, and C. C. Landry (2012), Dust radiative forcing in snow of the Upper Colorado River Basin: 2. Interannual variability in radiative forcing and snowmelt rates, *Water Resour. Res.*, *48*, W07522, doi:10.1029/2012WR011986.

Sterle, K. M., J. R. McConnell, J. Dozier, R. Edwards, and M. G. Flanner (2013), Retention and radiative forcing of black carbon in eastern Sierra Nevada snow, *Cryosphere*, *7*, 365–374, doi:10.5194/tc-7-365-2013.

Sturm, M., and C. S. Benson (1997), Vapor transport, grain growth and depth-hoar development in the subarctic snow, *J. Glaciol.*, *43*(143), 42–59.

Sun, S., J. Jin, and Y. Xue (1999), A simple snow-atmosphere-soil transfer model, *J. Geophys. Res.*, *104*(D16), 19,587–19,597, doi:10.1029/1999JD900305.

Thompson, L. G., T. Yao, E. Mosley-Thompson, K. A. Henderson, and P. N. Lin (2000), A high-resolution millennial record of the south Asian monsoon from Himalayan ice cores, *Science*, *289*, 1916–1919, doi:10.1126/science.289.5486.1916.

Toon, O. B., C. P. McKay, T. P. Ackerman, and K. Santhanam (1989), Rapid calculation of radiative heating rates and photodissociation rates in inhomogeneous multiple scattering atmospheres, *J. Geophys. Res.*, *94*(D13), 16,287–16,301, doi:10.1029/JD094iD13p16287.

Warren, S. G., and W. J. Wiscombe (1980), A model for the spectral albedo of snow. II: Snow containing atmospheric aerosols, *J. Atmos. Sci.*, *37*, 2734–2745, doi:10.1175/1520-0469(1980)037<2734:AMFTSA>2.0.CO;2.

Wiscombe, W. J., and S. G. Warren (1980), A model for the spectral albedo of snow. I: Pure snow, *J. Atmos. Sci.*, *37*, 2712–2733, doi:10.1175/1520-0469(1980)037<2712:AMFTSA>2.0.CO;2.

Xu, B. Q., et al. (2009), Black soot and the survival of Tibetan glaciers, *Proc. Natl. Acad. Sci. U.S.A.*, *106*(52), 22,114–22,118, doi:10.1073/pnas.0910444106.

Xue, Y., P. J. Sellers, J. L. Kinter, and J. Shukla (1991), A simplified model for global climate studies, *J. Clim.*, *4*, 345–364, doi:10.1175/1520-0442(1991)004<0345:ASBMFG>2.0.CO:2.

Xue, Y., F. J. Zeng, K. Mitchell, Z. Janjic, and E. Rogers (2001), The impact of land surface processes on the simulation of the U.S. hydrological cycle: A case study of 1993 US flood using the Eta/SSiB regional model, *Mon. Weather Rev.*, *129*, 2833–2860, doi:10.1175/1520-0493(2001)129<2833:TIOLSP>2.0.CO;2.

Xue, Y., S. Sun, D. S. Kahan, and Y. Jiao (2003), Impact of parameterizations in snow physics and interface processes on the simulation of snow cover and runoff at several cold region sites, *J. Geophys. Res.*, *108*(D22), 8859, doi:10.1029/2002JD003174.

Xue, Y., R. Vasic, Z. Janjic, F. Mesinger, and K. E. Mitchell (2007), Assessment of dynamic downscaling of the continental U.S. regional climate using the Eta/SSiB Regional Climate Model, *J. Clim.*, *20*, 4172–4193, doi:10.1175/JCLI4239.1.

Yang, F., A. Kumar, W. Wang, H.-M. H. Juang, and M. Kanamitsu (2001), Snow-albedo feedback and seasonal climate variability over North America, *J. Clim.*, *14*, 4245–4248, doi:10.1175/1520-0442(2001)014<4245:SAFASC>2.0.CO;2.

Zhang, W., and J. H. Scneibel (1995), The sintering of two particles by surface diffusion and grain boundary diffusion—A two-dimensional numerical study, *Acta Metall. Mater.*, *43*(12), 4377–4386, doi:10.1016/0956-7151(95)00115-C.

Zhao, C., et al. (2014), Simulating black carbon and dust and their radiative forcing in seasonal snow: A case study over North China with field campaign measurements, *Atmos. Chem. Phys.*, *14*, 11,475–11,491, doi:10.5194/acp-14-11475-2014.